© 2021. Published by The Company of Biologists Ltd | Development (2021) 148, dev196345. doi:10.1242/dev.196345

STEM CELLS AND REGENERATION

RESEARCH ARTICLE

The exocyst complex regulates *C. elegans* germline stem cell proliferation by controlling membrane Notch levels

Kumari Pushpa[1,‡], Sunayana Dagar[1,2,*], Harsh Kumar[1,3,*], Diksha Pathak[1] and Sivaram V. S. Mylavarapu[1,2,3,‡]

ABSTRACT

The conserved exocyst complex regulates plasma membrane-directed vesicle fusion in eukaryotes. However, its role in stem cell proliferation has not been reported. Germline stem cell (GSC) proliferation in the nematode *Caenorhabditis elegans* is regulated by conserved Notch signaling. Here, we reveal that the exocyst complex regulates *C. elegans* GSC proliferation by modulating Notch signaling cell autonomously. Notch membrane density is asymmetrically maintained on GSCs. Knockdown of exocyst complex subunits or of the exocyst-interacting GTPases Rab5 and Rab11 leads to Notch redistribution from the GSC-niche interface to the cytoplasm, suggesting defects in plasma membrane Notch deposition. The anterior polarity (aPar) protein Par6 is required for GSC proliferation, and for maintaining niche-facing membrane levels of Notch and the exocyst complex. The exocyst complex biochemically interacts with the aPar regulator Par5 (14-3-3ζ) and Notch in *C. elegans* and human cells. Exocyst components are required for Notch plasma membrane localization and signaling in mammalian cells. Our study uncovers a possibly conserved requirement of the exocyst complex in regulating GSC proliferation and in maintaining optimal membrane Notch levels.

KEY WORDS: Exocyst complex, Germline stem cells, Notch, Intracellular trafficking, Par proteins

INTRODUCTION

Intracellular vesicular trafficking is essential for various cellular processes such as growth, migration, division, signaling and maintaining polarity (Clague and Urbé, 2001; Liu and Guo, 2012; Maritzen et al., 2015; McKay and Burgess, 2011; Polgar and Fogelgren, 2018; Tojima and Kamiguchi, 2015). The exocyst complex is an evolutionarily conserved, octameric-protein complex containing the subunits Sec3, Sec5, Sec6, Sec8, Sec10, Sec15, Exo70 and Exo84 (Mei et al., 2018), which regulates the polarized targeting and plasma membrane fusion of Golgi-derived secretory vesicles and recycling endosomes (He and Guo, 2009; Heider and Munson, 2012; Wu and Guo, 2015; Zhu et al., 2017).

The nematode *Caenorhabditis elegans* is an excellent model for studying intracellular trafficking, wherein several components of the secretory pathway are important for viability and fertility (Hanna et al., 2013). Knockdown of exocyst complex subunits results in embryonic and larval lethality (Armenti et al., 2014; Chen et al., 2014b). The exocyst complex is required for seamless tube formation in the excretory cell (Armenti et al., 2014; Lant et al., 2015), for anchor cell invasion during vulval development (Naegeli et al., 2017) and for dendritic branching (Taylor et al., 2015; Zou et al., 2015). The role of vesicular trafficking in germline development is beginning to be appreciated (Hubbard and Greenstein; Pazdernik and Schedl, 2013; Green et al., 2011; Hanna et al., 2013; Pal et al., 2017). Tethering complexes such as TRAPP (transport protein particle) and COG (conserved oligomeric Golgi) have been reported to function in *C. elegans* development (Green et al., 2011; Hanna et al., 2013). However, the role of the exocyst complex in germline development, especially in germline stem cell proliferation, and more generally in stem cells, has not been reported.

Adult *C. elegans* hermaphrodites possess two U-shaped gonads, each open at one end to the uterus while the closed end houses the mitotically proliferating germline stem cells (GSCs), enwrapped by their somatic niche, the distal tip cell (DTC) (Hubbard and Greenstein, 2005). Stem cells start differentiating to form gametes as they exit the physical reach of the niche. Mitotic proliferation of GSCs requires the evolutionarily conserved, canonical Notch (GLP-1)-Delta (LAG-2) signaling (Kimble et al., 1992), which is known to function in stem cell proliferation and cell fate determination in a variety of developmental contexts, and is also over-expressed in several cancers (Artavanis-Tsakonas et al., 1999; Gridley, 2003; Liu et al., 2010; Siebel and Lendahl, 2017). Vesicular trafficking plays a crucial role in regulating Notch signaling in both signal-sending (Delta ligand containing) and signal-receiving (Notch receptor containing) cells (Barth and Köhler, 2014; Kandachar and Roegiers, 2012; Schnute et al., 2018; Yamamoto et al., 2010). In *Drosophila*, exocyst complex members are required for recycling of Delta during the asymmetric division of sensory organ precursors (Jafar-Nejad et al., 2005), and for Notch trafficking during egg chamber development during oogenesis (Wan et al., 2019). The exocyst complex has otherwise not been implicated in regulating Notch signaling in any system.

Here, we report a novel requirement for the exocyst complex in GSC proliferation and regulating Notch (GLP-1) trafficking to the GSC-niche interface. RNAi of exocyst components reduces GSC proliferation, while epistasis analysis suggests that the exocyst complex promotes Notch/GLP-1 signaling in the germline. Surprisingly, GLP-1 is asymmetrically localized on the GSC membrane. Knockdown of exocyst complex subunits leads to lower membrane Notch levels and reduced Notch-Delta signaling in GSCs and in mammalian cells. The exocyst complex and Notch interact in both *C. elegans* and mammalian cells, suggesting a conserved role of the exocyst complex in intracellular Notch trafficking. We found that the aPar complex and PAR-5/14-3-3ζ modulate GLP-1

[1]Laboratory of Cellular Dynamics, Regional Centre for Biotechnology, NCR Biotech Science Cluster, 3rd Milestone Faridabad-Gurgaon Expressway, Faridabad, Haryana 121001, India. [2]Kalinga Institute of Industrial Technology, Bhubaneswar, Odisha 751024, India. [3]Manipal Academy of Higher Education, Manipal, Karnataka 576104, India.
*These authors contributed equally to this work

‡Authors for correspondence (sivaram@rcb.res.in; pushpakumari81@gmail.com)

K.P., 0000-0002-0230-4177; S.D., 0000-0002-5070-9232; H.K., 0000-0003-2384-2115; S.V.S.M., 0000-0001-5990-1362

Handling Editor: Swathi Arur
Received 27 August 2020; Accepted 30 June 2021

Development (2021) 148, dev196345. doi:10.1242/dev.196345

localization in GSCs and that PAR-6 is required for engagement of the exocyst subunit SEC-6 to the GSC membrane. Finally, we identified a novel biochemical interaction between SEC-6/Exoc3 and PAR-5/14-3-3ζ in *C. elegans* and mammalian cells. Our results uncover the regulation of stem cell proliferation by the exocyst complex, possibly by regulating Notch signaling, and suggest the evolutionary conservation of the exocyst-Notch crosstalk in stem cell systems.

RESULTS

The exocyst complex is required for proliferation of germ cells in the progenitor zone

Multiple exocyst complex members have been reported to be required for various cellular and development processes in *C. elegans*, such as lumenogenesis (Armenti et al., 2014; Lant et al., 2015), dendritic outgrowth (Taylor et al., 2015; Zou et al., 2015), stem cell niche plexus maintenance (Linden et al., 2017) and intracellular trafficking in intestinal cells (Chen et al., 2014b). Genetic mutants of a few exocyst components are sterile (Armenti et al., 2014; Chen et al., 2014b), but their role in germline development is unknown. We examined the role of *C. elegans* exocyst complex subunits SEC-6 and its partner SEC-8 in germline development. The *sec-6* mutant allele *tm4536* was lethal at the L1 stage; we therefore relied on RNAi to knockdown *sec-6* (as reported previously, Kumar et al., 2019) or *sec-8*, which also led to significant F1 embryonic and larval lethality (Fig. 1A), although a few animals were viable and survived to adulthood.

Knockdown of *sec-6* or *sec-8* resulted in fertility defects in the F1 generation (>50% animals) (Fig. 1B), while even the fertile animals produced fewer progeny (Fig. 1C). Dissected and DAPI-stained gonads from both *sec-6*- and *sec-8*-depleted worms showed a smaller progenitor zone (PZ), with both the PZ length and the total number of GSCs reduced when compared with the control RNAi (Fig. 1E-G). RNAi of *sec-6* and *sec-8* also caused significant endoreduplication during oogenesis (Fig. 1D,E). In lieu of a viable genetic mutant, a near-complete removal of *sec-6* gene activity was achieved by *sec-6* RNAi on the heterozygous *sec-6*(*tm4536/hT2*) animals, which displayed a similarly small-sized PZ, confirming an efficient RNAi in the wild-type background (Fig. 1H,I, Fig. S1). We also examined the germline in the *sec-8(ok2187)* animals that had earlier been reported to be sterile (Armenti et al., 2014). Similar to the *sec-8* (RNAi) phenotype, *sec-8(ok2187)* worms showed a significantly smaller PZ when compared with wild type (N2) and *sec-8(ok2187/hT2)* (Fig. S1). Immunostaining for WAPL-1, a bona fide PZ marker, revealed reduced GSC numbers in both *sec-8(ok2187)* and *sec-8(ok2187/hT2)* when compared with wild type (Fig. 1J-L) (Kocsisova et al., 2019). As the overall RNAi phenotypes (Fig. 1E,G) were similar to the phenotypes of the genetic mutants (Fig. 1F,H-K, Fig. S1), we used RNAi-mediated knockdown of *sec-6* and *sec-8* for the rest of the study.

The smaller PZ was likely due to a germ cell proliferation defect. Immunostaining for phosphorylated histone 3 (PH3), a marker for actively dividing germ cells, revealed a ∼45% reduction in the mitotic index upon *sec-6/sec-8* RNAi in comparison with control animals (Fig. 2A-C). To confirm the role of other exocyst subunits in germline development, we tested mutants of *sec-3(ok3591)* and *sec-5(pk2358)*. Mutants for *sec-3* were not viable, so could not be analyzed and the germline of *sec-5* mutant did not show any discernible phenotype (Fig. S2). However, a further RNAi of *sec-3* and *sec-5* on the respective mutant backgrounds resulted in a phenocopy of *sec-6* RNAi (Fig. 1, Fig. S1). Taken together, the above results suggest that the exocyst complex subunits SEC-3-SEC-5-SEC-6-SEC-8 play important roles in germline development in *C. elegans*, specifically in germ cell proliferation.

The exocyst complex functions in both the germline and the soma to regulate GSC divisions

Germ cells in *C. elegans* are present in an intimate network of multiple types of somatic cells (DTC, sheath cells and uterine tissue), which together provide a conducive environment for their proliferation and differentiation. A few earlier studies and the data from The Nematode Expression Pattern Database (NEXTDB) suggest that the exocyst complex localizes to both germ cells and DTC (Armenti et al., 2014; Linden et al., 2017). To gain clarity in this aspect, we examined the protein expression of exocyst subunits in germ cells. A transgenic line containing SEC-6::GFP::SBP generated in our earlier study (Kumar et al., 2019) showed expression in the germ cell cytoplasm, including the oocytes (Fig. 2D). Fluorescently tagged SEC-5 and SEC-15 generated in an earlier study (Armenti et al., 2014) also displayed germline expression similar to SEC-6::GFP (Fig. S3A). We also observed the expression of SEC-6::GFP in the DTC cytoplasm (Fig. 2E). To test whether the exocyst complex functions in a germline-autonomous manner, we used *rrf-1(ok589)* and *ppw-1(pk2505)* mutants, which restrict RNAi to germline and somatic cells, respectively (Kumsta and Hansen, 2012; Tijsterman et al., 2002). Knockdown of *sec-6* or *sec-8* in both *rrf-1(ok589)* and *ppw-1(pk2505)* mutants resulted in a significantly smaller PZ and fewer GSCs (Fig. 2F,G). We further confirmed our observations using germline-specific rescue of *rde-1(mkc36)* [sun-1p::rde-1 (DCL569)], which allows only germline-specific RNAi. Knockdown of *sec-6* or *sec-8* on the *sun-1p::rde-1*; *rde-1(mkc36)* background also resulted in marked reduction in GSC number (Fig. 2H). Additionally, a significant number of gonads also displayed endoreduplicating oocytes in both *rrf-1(ok589)* and *sun-1p::rde-1*; *rde-1(mkc36)* backgrounds when compared with control RNAi (Fig. S1C,D). We specifically degraded SEC-6 in the germline using an auxin-inducible degradation (AID) system by generating a transgenic line expressing SEC-6::degron-tag at the endogenous locus by CRISPR-CAS9-mediated editing and combining it with germline-expressed transgenic TIR1. A 48 h treatment with 2 mM auxin at the L4 stage resulted in moderate reduction of SEC-6 expression, as revealed by immunoblots from whole-worm lysates (Fig. 2I); these animals displayed a smaller PZ similar to *sec-6* RNAi on *rrf-1* and *sun-1p::rde-1*; *rde-1(mkc36)* backgrounds (Fig. 2F,G). When combined, these observations strongly support a germline-autonomous function of the exocyst complex, in addition to its role in somatic cells, for germline development in *C. elegans*.

The exocyst complex promotes Notch signaling for germline stem cell proliferation

Proliferation of GSCs in the progenitor zone is dependent on canonical Notch-Delta signaling (Kimble and Crittenden, 2005), the loss of which results in sterility due to depletion of the GSC pool (Kimble and Crittenden, 2005). To ascertain whether the exocyst complex regulates Notch signaling in germ cells, we used genetic epistasis of exocyst components with temperature-sensitive *glp-1* mutant alleles *bn18* (loss of function) and *ar202* (gain of function) (Austin and Kimble, 1987; Kodoyianni et al., 1992; Pepper et al., 2003). At the restrictive temperature (23-25°C), *glp-1(ar202)* worms develop germline tumors due to uncontrolled GSC proliferation (Fig. 3A); however, knockdown of *sec-6* or *sec-8* completely inhibited tumor formation in a significant number of animals

Development (2021) 148, dev196345. doi:10.1242/dev.196345

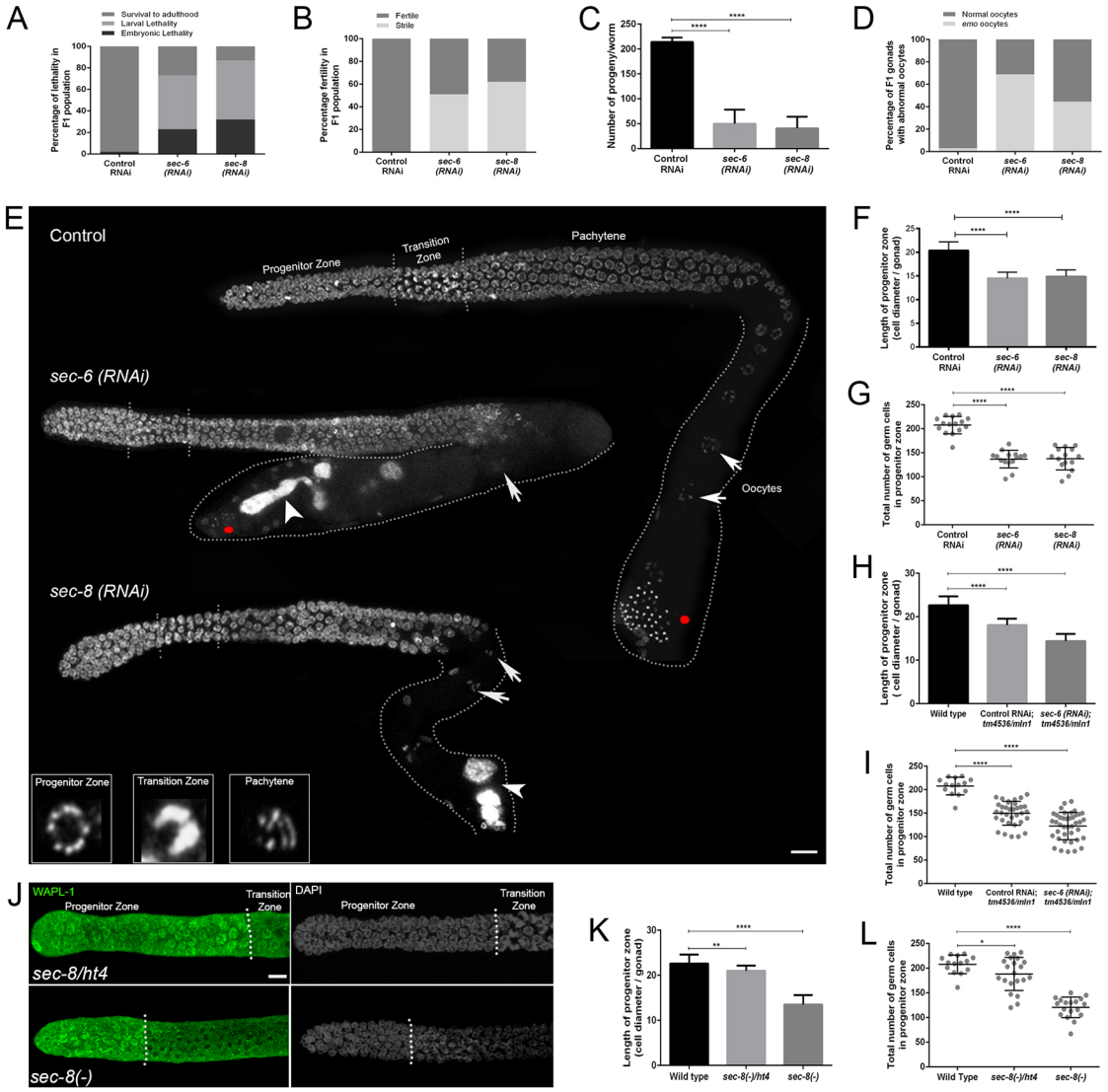

Fig. 1. The exocyst complex is required for germline development in *C. elegans*. (A-C) Progeny of F0 animals depleted of exocyst complex subunits *sec-6* and *sec-8* (*n*=12 for each genotype) were analyzed in comparison with control RNAi for survival, fertility and brood size. The bar graphs show the percentage of (A) lethality and (B) fertility in the F1 population, and (C) the number of progeny produced by fertile F1 animals (*n*=12 for each genotype). (D) Percentage of gonads in F1 animals (*n*=85 for each genotype) with endoreduplicating oocytes upon RNAi of exocyst complex subunits. (E) Representative images of dissected hermaphrodite gonads stained with DNA-binding dye (DAPI, gray) upon the indicated RNAi. The transition zone (TZ) is distinguished from the mitotic and meiotic ('pachytene') zones by dashed lines. Arrows indicate oocytes, solid red dots indicate the sperm and arrowheads show endoreduplicating oocytes (Emo). Insets each show a magnified representative germ cell nucleus from PZ, TZ and pachytene. Scale bar: 20 µm; 2.5 µm in the insets. (F,H,K) The length of the PZ counted as germ cell diameter (*n*=at least 20/22/15 gonads, respectively) in the indicated genotypes. (G,I, L) Total number of germ cells in the PZ (*n*=at least 15/23/14 gonads, respectively) in the indicated genotypes. (J) Representative confocal immunofluorescence micrographs of dissected hermaphrodite gonads from the indicated genetic mutants stained using anti-WAPL-1 antibody (green) and DNA-binding dye (gray, DAPI). Dashed line separates the WAPL-1-positive PZ from the TZ. Scale bar: 10 µm. The same data for wild type was used for analysis in H-L. Data are mean±s.d. **P*<0.05, ***P*<0.01, *****P*<0.0001.

(Fig. 3A,B). The loss-of-function *glp-1(bn18)* mutant normally displays a smaller PZ at the permissive temperature (15-20°C), and a complete loss of GSCs at the elevated temperatures (23-25°C). Upon *sec-6* or *sec-8* RNAi in the *glp-1(bn18)* background at 20°C, we observed a further reduction in PZ length when compared with *glp-1(bn18)* (Fig. 3C,D). Thus, knockdown of exocyst subunits inhibited tumor formation in the gain-of-function mutant, and enhanced the severity of the loss-of-function mutant, indicating a positive genetic interaction between the exocyst complex and Notch/GLP-1 signaling either by working in the same pathway or parallel to it. To delineate this further, we used two genetic mutants, namely *gld-2(q497);gld-1(q361)* and *gld-3(q730);nos-3(q650)*, which disrupt the meiotic entry/differentiation pathway and form Notch-independent germline tumors (Kadyk and Kimble, 1998; Hansen et al., 2004). Knockdown of *sec-6* failed to affect these tumors (Fig. 3E), supporting a model of exocyst complex function in GSC proliferation via Notch/GLP-1-dependent pathway.

We confirmed the effect of the exocyst complex on Notch signaling by determining the expression of GLD-1, a germ cell differentiation marker negatively regulated by Notch-Delta signaling in control and exocyst complex RNAi (Brenner and Schedl, 2016; Hansen et al., 2004; Suh et al., 2009). In wild-type worms, GLD-1 expression increases gradually around 10-12 germ cell diameters (GCDs) from the distal end of the gonad, before peaking as germ cells

Development (2021) 148, dev196345. doi:10.1242/dev.196345

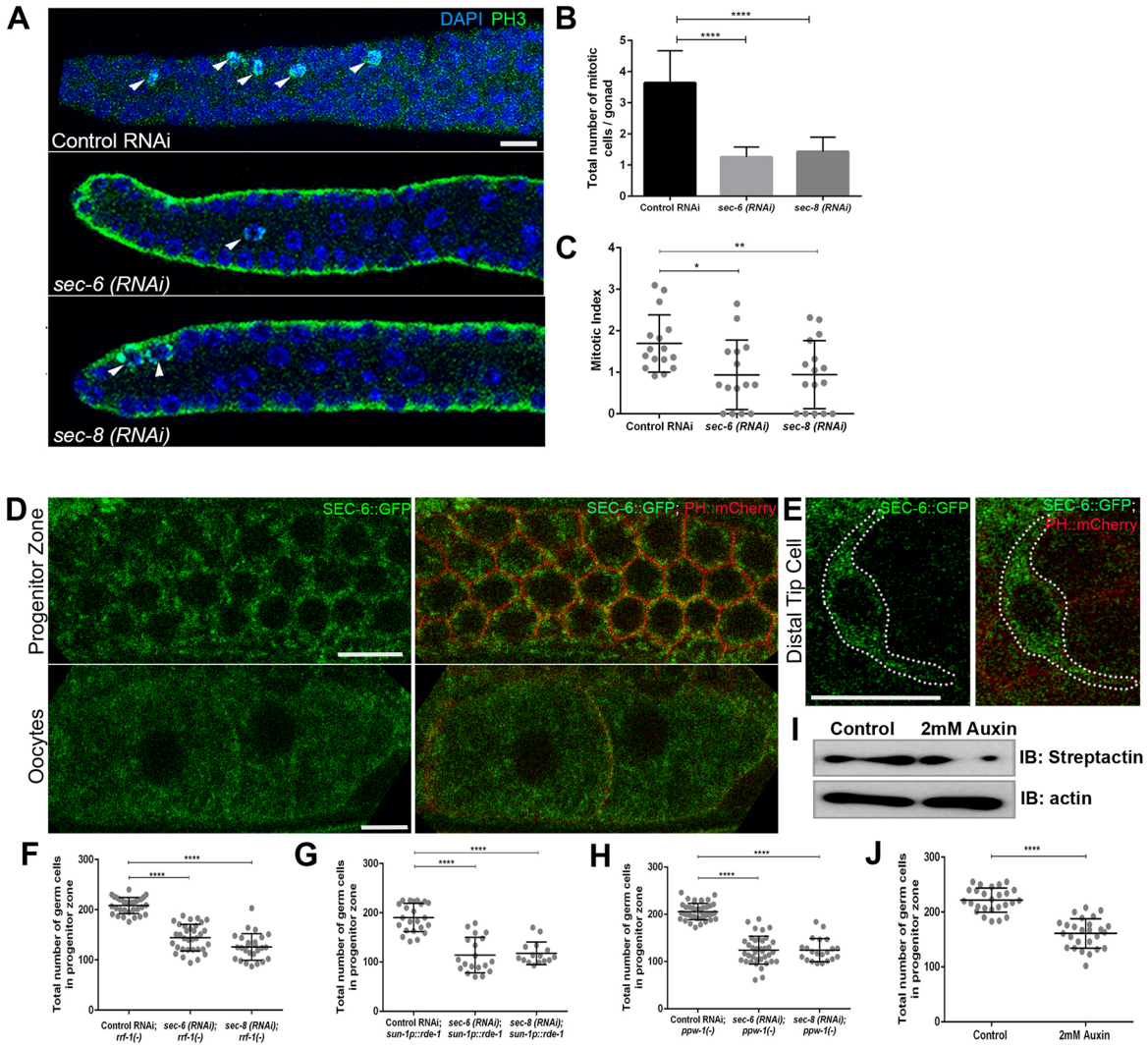

Fig. 2. The exocyst complex functions in the germline to promote germ cell proliferation. (A) Image showing the distal region of the dissected gonads of the respective genotypes stained with the indicated antibody/dye. Arrowheads indicate metaphase or anaphase germ cell nuclei. (B) Number of phosphohistone 3 (PH3)-positive germ cells per gonad in the indicated RNAi; *n*=37 (control RNAi), 41 (*sec-6 RNAi*) and 46 (*sec-8 RNAi*). (C) Scatter plot showing the mitotic index (number of PH3-positive cells as a fraction of total cells in the PZ) in the respective genotypes; each dot indicates one gonad; *n*=16 (control RNAi), 15 (*sec-6 RNAi*) and 16 (*sec-8 RNAi*). (D) Representative images showing expression of SEC-6::GFP at the endogenous loci in germ cells of the PZ and oocytes. (E) Representative confocal fluorescence micrographs showing SEC-6::GFP expression in the DTC (boundary marked by dotted line). (F-H) Total number of GSCs observed after exocyst subunit RNAi in the *rrf-1* mutant (F), *sun-1p::rde-1* (G, germline specific) and *ppw-1* mutant (H, soma specific); *n*>32 (control RNAi), >33 (*sec-6 RNAi*) and >25 (*sec-8 RNAi*). (I) Immunoblots from animals expressing SEC-6::degron::GFP::SBP treated with control and 2 mM auxin for 48 h using antibody against SBP-tag. (J) Total number of GSCs 48 h post-treatment with control and 2 mM auxin. Scale bars: 10 µm. Data are mean±s.d. **P*<0.05, ***P*<0.01, *****P*<0.0001.

enter meiosis around 19-20 GCDs (Fig. 3E) (Brenner and Schedl, 2016). After exocyst subunit RNAi, the level of GLD-1::GFP increased overall when compared with control RNAi, and was precociously expressed even in GSCs at 8-10 GCDs from the distal end (Fig. 3E,F). We also analyzed the direct downstream targets of GLP-1 signaling in GSCs, i.e. LST-1 and SYGL-1 (Kershner et al., 2014), using their respective V5-tagged transgenic strains (Shin et al., 2017). Upon RNAi of *sec-6* or *sec-8*, we observed a halving in LST-1::V5 expression levels (Fig. 3G,I), with 30-40% less GSCs expressing LST-1 when compared with control RNAi (Fig. 3H); a similar reduction in SYGL-1::V5 expression was also observed upon *sec-6* RNAi (Fig. 3J-L). Collectively, these results suggest a positive genetic interaction between the exocyst complex and Notch signaling in GSCs, measured using both direct and indirect targets of the signaling pathway.

The exocyst complex is required for proper trafficking in the germline

Exocyst complex function has been demonstrated in membrane trafficking in both the soma and the germline of *C. elegans* (Armenti et al., 2014; Chen et al., 2014b; Jiu et al., 2014, 2012; Zou et al., 2015; Balklava et al., 2007). Vesicular trafficking is essential for proper oocyte maturation (Grant and Sato, 2006; Hanna et al., 2013; Sato et al., 2014). Yolk secreted from the intestine into the body cavity is endocytosed by maturing oocytes (Grant and Sato, 2006). We examined yolk uptake in oocytes using mCherry-tagged yolk protein YP170 (Grant and Hirsh, 1999). An endocytic block accumulates YP170 in the body cavity, while a secretion block results in intestinal accumulation (Grant and Hirsh, 1999). RNAi of *sec-6* or *sec-8* led to significant YP170 accumulation in the body cavity, indicating defective endocytosis of yolk proteins (Fig. 4A).

Development (2021) 148, dev196345. doi:10.1242/dev.196345

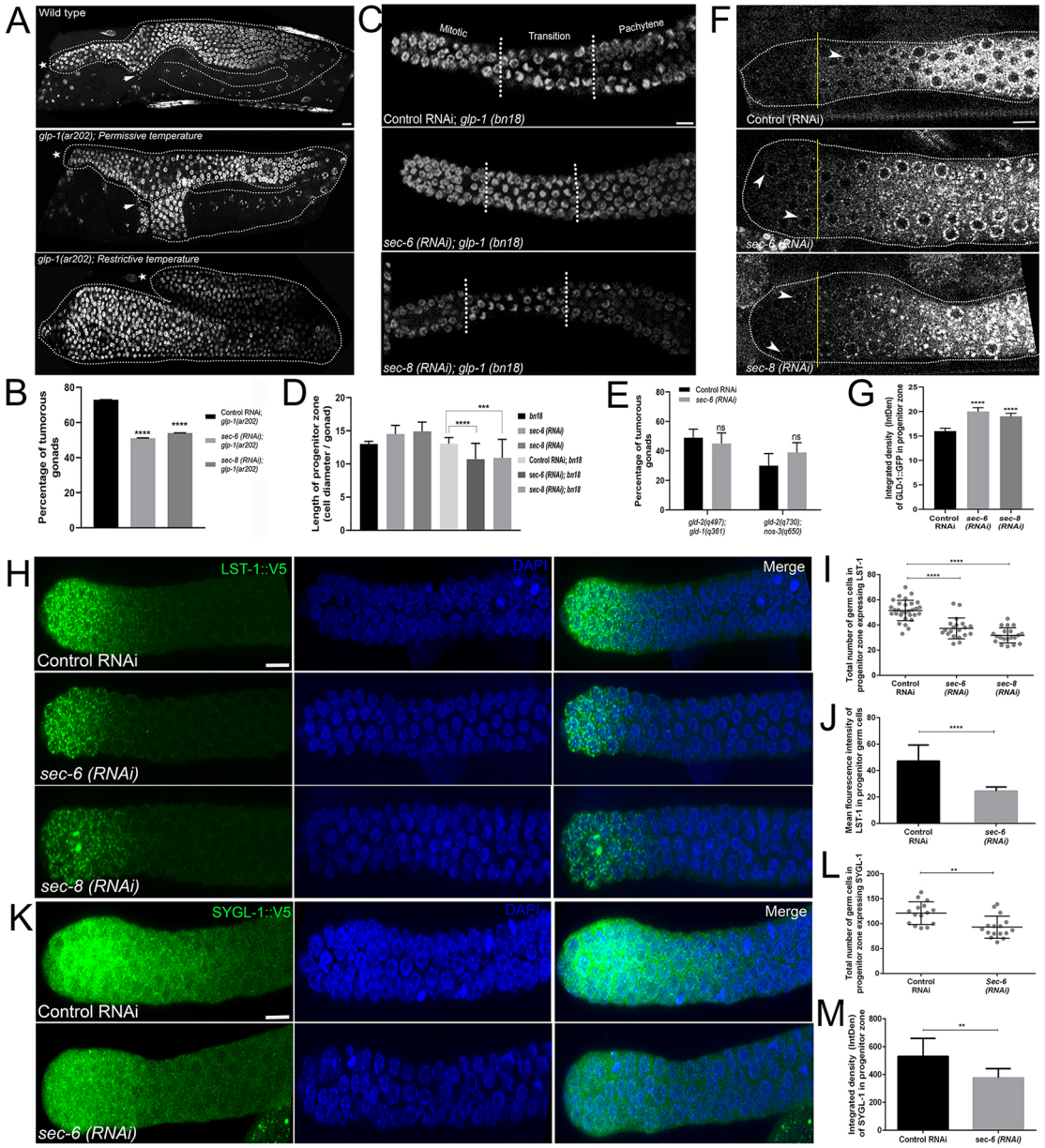

Fig. 3. The exocyst complex promotes Notch signaling in GSCs. (A) Representative fluorescence micrographs of whole-mount worms displaying gonads stained with DAPI (gray) in the respective genotypes. The proximal end of the gonad shows uncontrolled tumor growth at the restrictive temperature (lowest panel). Asterisk, distal end; arrow, sperm. Scale bar: 20 µm. (B,E) Fraction of tumorous gonads in the indicated genotypes: Notch-dependent (B) and Notch-independent (E) tumors; *n*>200 worms per genotype. (C) Representative images of dissected hermaphrodite gonads of the indicated genotypes stained with DAPI (gray). Dotted lines demarcate the PZ and TZ. Scale bar: 10 µm. (D) Length of the PZ in the indicated genotypes; data for *sec-6(RNAi)* and *sec-8(RNAi)* is the same as that used in Fig. 1F. *n*≥40 gonads for each genotype. (F) Representative confocal fluorescence micrographs of the PZ of the gonad showing expression of GLD-1::GFP (gray) in the indicated genotypes. Yellow line marks the beginning of the expression of GLD-1 in the PZ in control worms; arrowheads indicate precocious expression. Scale bar: 10 µm. (G) Bar chart representing the integrated fluorescence density of GLD-1::GFP (corrected for background fluorescence) in the first 10 germ cell diameters (GCDs) from the distal end of the gonad; *n*=25 gonads in each genotype. (H,K) Representative anti-V5 (green) confocal immunofluorescence images of dissected adult hermaphrodite gonads from animals expressing LST-1::V5 (H) or SYGL1::V5 (K) upon control and exocyst subunit RNAi, as indicated. Scale bars: 10 µm. (I,L) Number of germ cells expressing LST-1::V5 (I) and SYGL-1:V5 (L) in the PZ. *n*>15 gonads for each genotype. (J,M) Mean integrated fluorescence density of LST-1::V5 (J) and SYGL-1:V5 (M) in the PZ upon the indicated exocyst subunit RNAi in comparison with control; *n*=15 for each genotype. Data are mean±s.d. ***P*<0.01, ****P*<0.001, *****P*<0.0001.

Knockdown of exocyst subunits also led to a significant accumulation of the yolk receptor RME-2 (Grant and Hirsh, 1999; Kang et al., 2011) underneath the oocyte membrane and as large aggregates in the cytoplasm (Fig. 4B, right panel, Fig. 4C, Fig. S5A), consistent with an earlier study reporting defects in yolk endocytosis and RME-2::GFP mislocalization upon *sec-6(RNAi)* (Balklava et al., 2007).

We further examined the localization of the recycling endosome marker RAB-11, of which the exocyst complex is an effector (Takahashi et al., 2012; van Ijzendoorn, 2006; Zhang et al., 2004). Exocyst subunit knockdown resulted in increased expression of RAB-11::GFP in oocytes (Fig. 4B, right panel, Fig. S5B). Fluorescence quantification revealed a ∼2- to 2.5-fold accumulation of RAB-11::GFP underneath the plasma membrane when compared

Development (2021) 148, dev196345. doi:10.1242/dev.196345

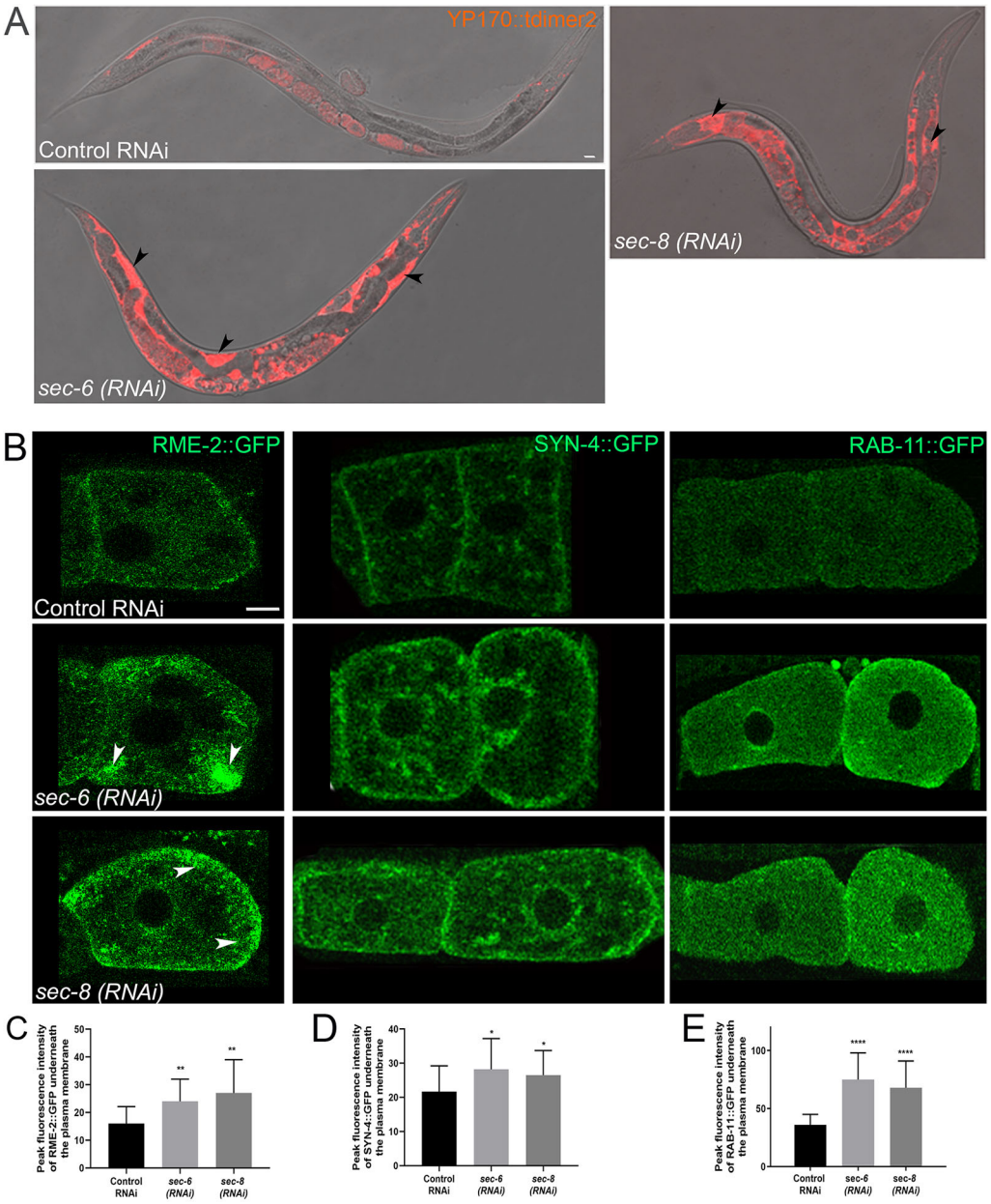

Fig. 4. The exocyst complex is required for intracellular trafficking in the germline. (A) DIC-fluorescence merged images of whole-mount *C. elegans* expressing yolk protein (YP170) tagged with mCherry (red) in the indicated genotypes. Scale bar: 20 µm. (B) Representative confocal fluorescence micrographs of mature oocytes expressing the yolk receptor RME-2::GFP, t-SNARE SYN-4::GFP and recycling endosome marker RAB-11::GFP in the indicated RNAi. Arrowheads indicate the sub-membrane accumulation of the fluorescence puncta. Scale bar: 10 µm. (C-E) Mean fluorescence intensity underneath the plasma membrane of the respective tagged proteins as indicated, measured by linescan analysis of confocal fluorescence micrographs. n>15 gonads per condition, two oocytes per gonad. Data are mean±s.d. *P<0.05, **P<0.01, ****P<0.0001.

with controls (Fig. 4E), possibly owing to the failure in plasma membrane fusion of RAB-11-positive recycling vesicles (Chen et al., 2014b). While the expression of *rab-11* mRNA by qRT-PCR was found to be about 20% higher than control (Fig. S4), this moderate increase alone does not account for the 2- to 2.5-fold increase in the membrane-proximal cytoplasmic accumulation of RAB-11. Together, our data suggest that exocyst complex subunit knockdown leads to a modest transcriptional upregulation of *rab-11*, leading to higher protein levels, as well as mislocalization underneath the plasma membrane.

The plasma membrane SNARE SYN-4 (SYX-4), a key component of the regulated plasma membrane-directed fusion machinery (Jantsch-Plunger and Glotzer, 1999), was also mislocalized underneath the plasma membrane upon exocyst subunit knockdown (Fig. 4B, central panel, Fig. 4D, Fig. S5C). Our qRT-PCR measurements of *rme-2* and *syn-4* mRNAs revealed a slight decrease in expression upon exocyst subunit knockdown, suggesting that mislocalization is unlikely due to altered mRNA expression (Fig. S4). When combined, these results confirm the role of the exocyst complex in vesicular trafficking in the germline, and point towards its function in targeting key trafficking components to the oocyte cell surface.

GLP-1 is asymmetrically localized in the germline

Intracellular trafficking is key for regulating Notch/GLP-1-Delta/LAG-2 signaling (Andersson et al., 2011; Kimble and Simpson, 1997). To test the hypothesis that the exocyst complex modulates Notch signaling in GSCs by regulating the intracellular trafficking of GLP-1, we obtained a GLP-1::GFP::3xFLAG-expressing strain and examined its distribution in GSCs. Similar to the endogenous GLP-1 expression, GLP-1::GFP was also largely localized to the GSC plasma membrane (Fig. 5A) (Ariz et al., 2009). Germ cells in the *C. elegans* gonad are membrane enclosed on three sides and open to a common lumen (rachis) on the fourth. Although not described as polarized cells, multiple proteins are distributed differentially in the rachis-facing ‘inner’ membrane and

Development (2021) 148, dev196345. doi:10.1242/dev.196345

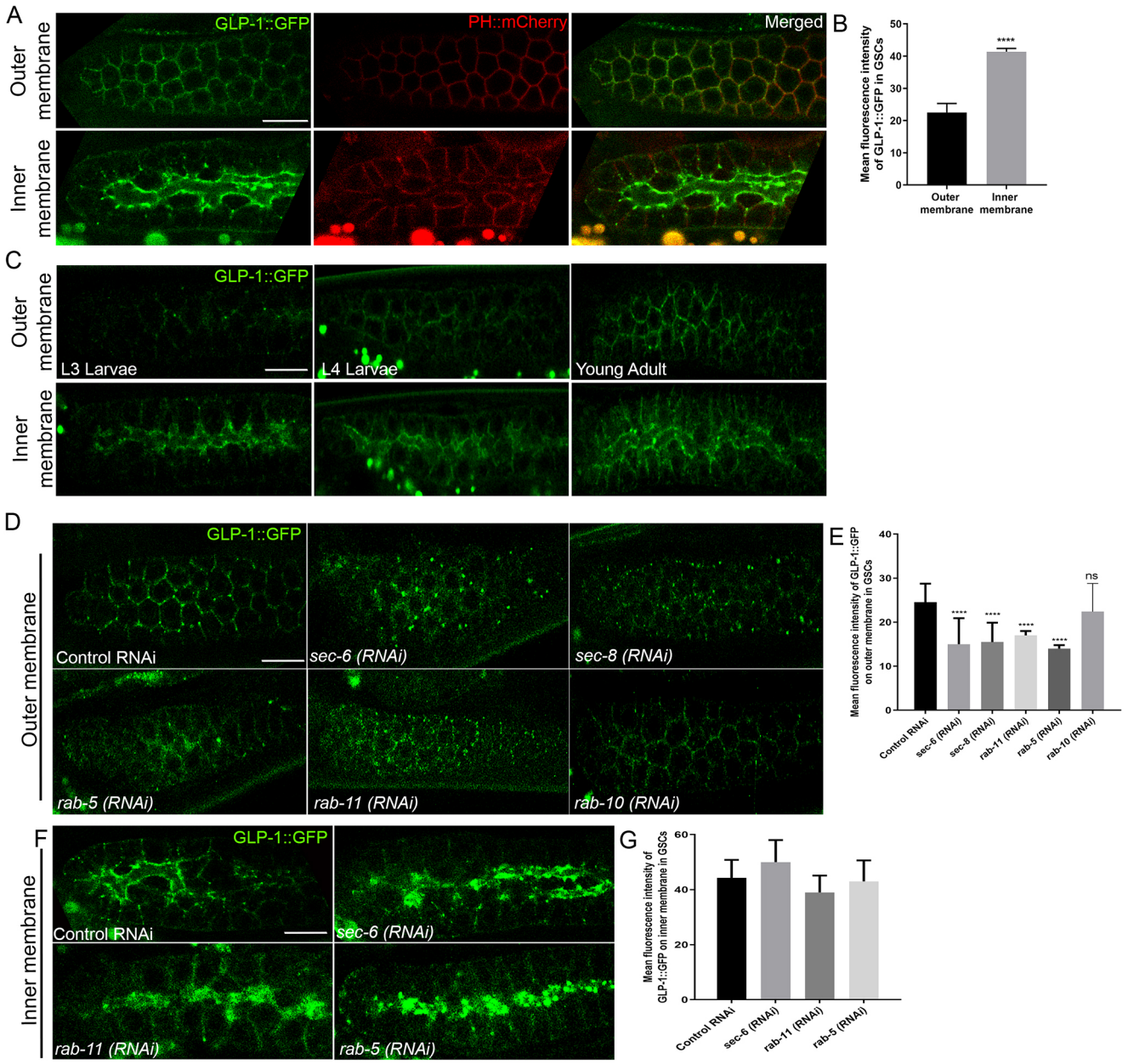

Fig. 5. Notch (GLP-1) localization in the GSCs is dependent on exocyst-, RAB-5- and RAB-11-mediated trafficking. (A) Representative confocal fluorescence micrographs of the PZ depicting the outer (signaling active) and the inner (signaling inactive) GSC plasma membranes from animals expressing GLP-1::GFP and PH::mCherry, as indicated. (B) Mean fluorescence intensity measurements of GLP-1::GFP on the outer and the inner membranes (see Materials and Methods); *n*=15 gonads, 150 cells. (C) Representative fluorescence micrographs of the PZ displaying the outer and the inner membranes, as indicated from animals expressing GLP-1::GFP at the indicated larval stages. (D,F) Representative confocal fluorescence micrographs showing GLP-1::GFP on the outer membrane (D) and inner membrane (F) of GSCs in the indicated genotypes. (E,G) Mean fluorescence intensity of GLP-1::GFP in the indicated genotypes on outer membrane (E) and inner membrane (G) measured by linescan analysis (see Materials and Methods), *n*=15 gonads, 100-150 cells in each genotype. Scale bars: 10 µm. Data are mean±s.d. ****P<0.0001; ns, non-significant.

niche-facing 'outer' membrane in germ cells (Amini et al., 2014; Maddox et al., 2005; Zhou et al., 2013). A detailed examination of GSCs using confocal microscopy revealed an asymmetric distribution of GLP-1::GFP on the membrane, with less receptor on the outer membrane and substantial enrichment on the inner membrane (Fig. 5A). Quantitative fluorescence imaging (Fig. S4, see Materials and Methods) in a strain expressing GLP-1::GFP and PH::mCherry (a membrane marker) revealed a 1.5- to 2-fold higher intensity of GLP-1::GFP on the inner membrane when compared with the outer membrane (Fig. 5B). A similar asymmetry in GLP-1 localization was observed in other larval stages (Fig. 5C). To confirm our observations, we used a validated strain expressing GLP-1 tagged with V5 epitope (GLP-1::V5) (Sorensen et al., 2020). Localization of GLP-1::V5 in the progenitor zone was also found to be similarly asymmetric across the outer and inner GSC membranes (Fig. S3B, upper panel), confirming the naturally unequal membrane distribution of GLP-1 in *C. elegans* GSCs.

Exocyst complex subunits and the small GTPases Rab5 and Rab11 are required for proper membrane localization of GLP-1

We next examined the role of the exocyst complex in regulating GLP-1 membrane localization in GSCs. RNAi of *sec-6* and *sec-8* resulted in

Development (2021) 148, dev196345. doi:10.1242/dev.196345

significantly reduced (~40%) localization of GLP-1::GFP at the outer membrane (Fig. 5D). However, a proportionate increase on the inner membrane was not apparent (Fig. 5F,G), rather GLP-1::GFP appeared to largely redistribute to the cytoplasm. We observed similar mislocalization of GLP-1::V5 levels from the outer membrane (Fig. S3B, bottom panel), confirming the role of the exocyst complex in regulating GLP-1 levels at the GSC-niche interface, without any perceptible defect in plasma membrane integrity (visualized by PH::GFP) upon RNAi of *sec-6* (Fig. S3C, bottom panel). We also observed significant mislocalization of GLP-1::GFP from the plasma membrane of oocytes upon exocyst subunit knockdown (Fig. S3C, top panel), suggesting that the exocyst complex is required for GLP-1 trafficking and proper membrane distribution in GSCs. Taken together with its requirement for GSC proliferation, our results suggest the possibility that GLP-1 trafficking by the exocyst complex regulates GSC proliferation by regulating its plasma membrane levels at the niche-facing interface.

Receptor endocytosis from the membrane is the initial step before eventual recycling to the surface. Members of the early endocytic pathway have been reported to be essential for Notch signaling in *Drosophila* (Fortini and Bilder, 2009). In addition, a crosstalk between the early endocytic machinery and the exocyst complex has also been reported (Boehm et al., 2017; Jose et al., 2015; Kumar et al., 2019; Sommer et al., 2005). We observed reduced GLP-1 localization on the outer GSC membrane upon RNAi of the early endocytic regulator RAB-5, similar to exocyst complex knockdown (Fig. 5D,E). In *Drosophila*, Rab11 and the exocyst subunit Sec15 are crucial for recycling Delta to the plasma membrane in the signal-sending cell of sensory organ precursors (Jafar-Nejad et al., 2005). A previous study in *C. elegans* intestinal cells (Chen et al., 2014b) and our own results (Fig. 4B) suggested a role for the exocyst complex in fusing RAB-11 vesicles to the plasma membrane. We therefore tested the role of *rab-11* in regulating GLP-1 trafficking in GSCs. Similar to *rab-5* and *sec-6* knockdown, *rab-11* RNAi led to reduced GLP-1 localization on the outer membrane (Fig. 5D,E). Both *rab-5* and *rab-11* RNAi resulted in a smaller PZ similar to exocyst subunit RNAi (Fig. S6). We did not observe significant mislocalization of GLP-1::GFP in GSCs upon RAB-10 RNAi (Fig. 5D,E), despite the exocyst complex being a RAB-10 effector in *C. elegans* (Chen et al., 2014b). Similar to *sec-6* RNAi, we did not observe any substantial changes in the inner GSC membrane levels of GLP-1::GFP upon either *rab-5* or *rab-11* knockdown (Fig. 5F,G). Together, these results implicate the GTPases RAB-5 and RAB-11 in GLP-1 trafficking and demonstrate that the outer membrane levels of GLP-1 in GSCs are regulated by the exocyst complex, RAB-5 and RAB-11.

Anterior Par proteins regulate exocyst complex-mediated GLP-1 trafficking

The Par ('partitioning') group of proteins are well-known mediators of polarity in several organisms (Lang and Munro, 2017; Nance and Zallen, 2011). Multiple reports suggest a functional interplay between Par proteins and the exocyst complex (Ahmed and Macara, 2017; Armenti et al., 2014; Das et al., 2014; Lalli, 2009). We explored whether the localization of GLP-1 in GSCs is dependent on Par proteins in addition to the exocyst complex. RNAi of the anterior Par (aPar) proteins PAR-6 or PAR-3 phenocopied the GLP-1::GFP mislocalization from the outer GSC membrane, as seen upon exocyst subunit RNAi; however, RNAi of PAR-2, the posterior Par protein, did not (Fig. 6A,B). *par-3*, *par-6* and *par-5* RNAi resulted in a smaller PZ similar to exocyst subunit RNAi (Fig. S6). Importantly, aPar proteins are required for recruitment of the exocyst complex to specific cell membrane regions in the *C. elegans* embryo (Armenti et al., 2014), and the exocyst subunit Exo84 interacts with Par6 in human neurons (Das et al., 2014). We examined the localization of SEC-6::GFP on the outer membrane in a transgenic strain carrying both SEC-6::GFP and PH::mCherry upon knockdown of *par-6*. The prominent localization of SEC-6::GFP underneath the outer plasma membrane observed in wild-type (Fig. 2C) and control RNAi worms was reduced by ~40% upon *par-6* RNAi (Fig. 6C,D). Similar to the *sec-6* RNAi, *par-6* knockdown resulted in enhanced accumulation of RAB-11::GFP beneath the outer GSC membrane (Fig. 6E,F). Notably, a role for aPar proteins in endocytic trafficking (Balklava et al., 2007) and its requirement for normal localization of RAB-11 vesicles has been reported earlier (Winter et al., 2012). In light of these studies, our results suggest the possibility that PAR-6 could modulate GLP-1 levels by regulating GLP-1 endocytosis, perhaps by engaging the exocyst complex at the GSC outer membrane.

To further understand the mechanism by which PAR-6 regulates the exocyst complex, we affinity purified SEC-6::GFP::SBP from whole-worm lysates, followed by mass spectrometric analysis to identify potential interaction partners; PH::GFP was used as the control. We identified multiple known interactors of SEC-6 (SEC-3, SEC-5, SEC-8 and RAB-11), thus validating the assay (Fig. S8, Table S3). Although aPar-complex proteins were not detected, we identified PAR-5 as a high-confidence potential interactor (12 peptides with 54.8% protein coverage). Additionally, we performed a genome-wide yeast two-hybrid screen using full length SEC-6 (1-796 amino acids) as the bait, against a *C. elegans* mixed-staged prey library (Hybrigenics, France). Interestingly, our screen identified PAR-5 as a highly likely interacting partner (confidence score: good) (Fig. S8). Immunoprecipitation of human Sec6/Exoc3 from U2OS cell lysates (osteosarcoma cell line) also revealed a specific interaction with 14-3-3ζ, the closest homolog of *C. elegans* PAR-5 (Fig. 6G). Importantly, the localization of GLP-1::GFP was also severely affected upon *par-5* RNAi in the GSCs (Fig. 6A), suggesting the functional relevance of this interaction. These results are significant in light of the known PAR-5/14-3-3ζ interaction with PAR-3 and its functional regulation of the aPar complex (Benton and St Johnston, 2003; Hurd et al., 2003), and the demonstrated role for PAR-5 in the localization of RAB-11-positive vesicles in the *C. elegans* intestine (Winter et al., 2012). To the best of our knowledge, these results reveal a novel, evolutionarily conserved interaction between Par5/14-3-3ζ and the exocyst complex.

The exocyst complex biochemically interacts with Notch and is required for its proper trafficking to the plasma membrane in mammalian cells

Both Notch signaling and exocyst complex-mediated vesicular trafficking are evolutionarily conserved across metazoans (Artavanis-Tsakonas et al., 1999; Heider and Munson, 2012). However, the role of the exocyst complex in Notch trafficking has not been reported in mammalian systems. We used U2OS cells, which display active Notch signaling (Yang et al., 2017), to investigate the requirement of the exocyst complex for Notch trafficking. Humans express four Notch proteins: Notch1-notch4 (Kopan and Ilagan, 2009). We screened for Notch localization using antibodies against Notch1, Notch2 and Notch4, and found Notch2 to be mostly localized on the plasma membrane (Fig. 7A,B). A combined siRNA-mediated knockdown of human Sec5, Sec6 and Sec8 (Fig. 7C) revealed perceptible mis-localization of Notch2 from the plasma membrane and from the perinuclear regions in comparison with the control (GFP siRNA) (Fig. 7A). Using the

Development (2021) 148, dev196345. doi:10.1242/dev.196345

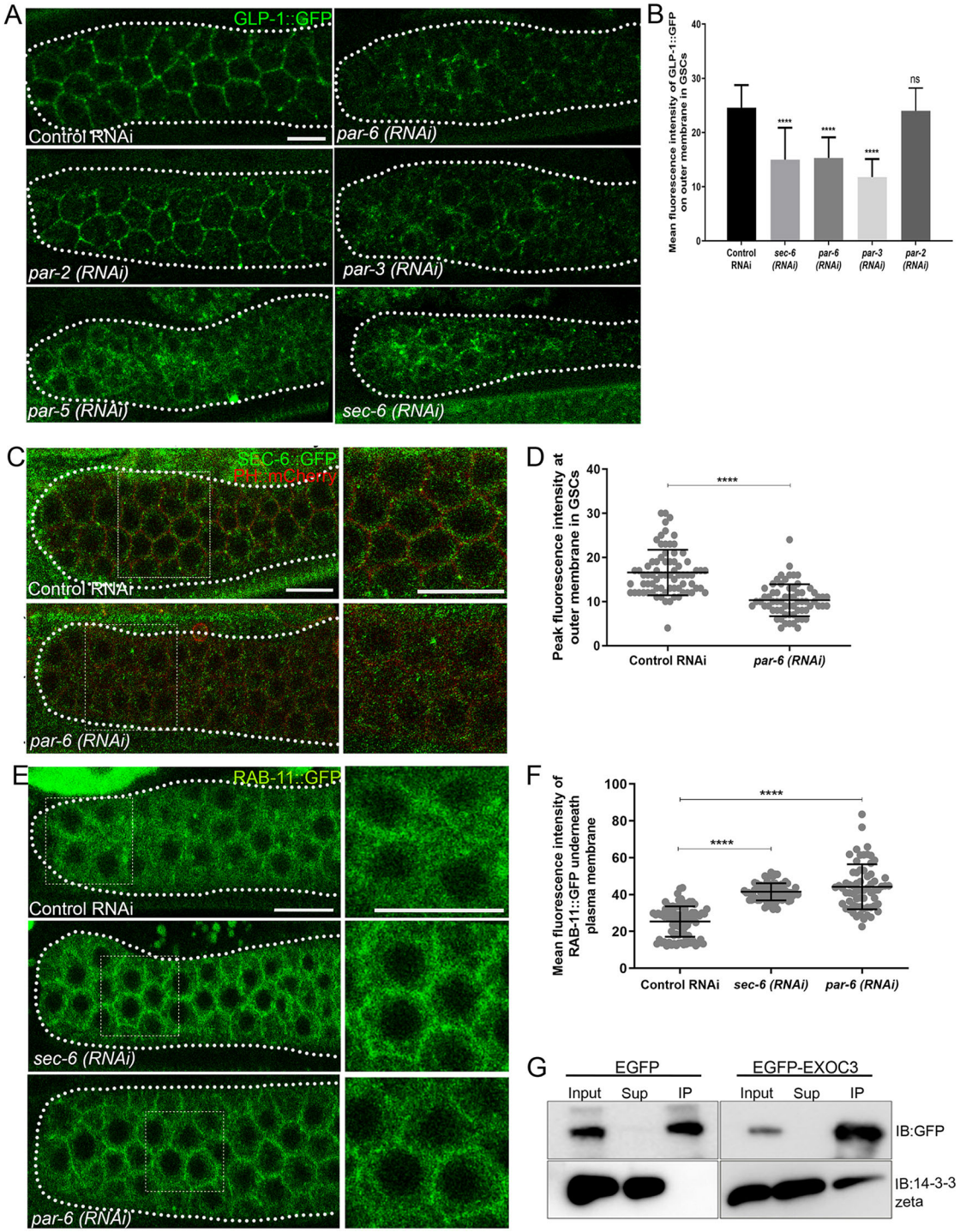

Fig. 6. The anterior Par complex maintains optimum Notch (GLP-1) levels on the GSC outer surface and regulates exocyst subunit localization. (A) Representative confocal fluorescence micrographs showing GLP-1::GFP localization at the outer GSC membrane in the indicated genotypes. (B) Mean fluorescence intensity of GLP-1::GFP on the outer GSC membrane in the respective genetic backgrounds as indicated; *n*=15 gonads, 120-150 cells for each genotype. (C) Localization of exocyst component SEC-6::GFP at/near the GSC outer membrane in the indicated genotypes. PH::mCherry marks the GSC plasma membrane. Right panels: digital zoom (twofold) of the regions outlined with a dashed square in the respective left panels. (D) Peak fluorescence intensity of GSC outer membrane-localized SEC-6::GFP in the indicated genotypes. *n*=15 gonads, 120-150 cells in each genotype. (E) Representative confocal fluorescence micrographs showing the localization of RAB-11::GFP underneath the GSC outer membrane in the indicated genotypes. Right panels: digital zoom (twofold) of the regions outlined with a dashed square in the respective left panels. (F) Mean fluorescence intensity of RAB-11::GFP underneath the outer GSC membrane in the indicated genotypes. *n*=12 gonads, 90-120 cells in each genotype. (G) Immunoblots of anti-GFP immunoprecipitates of EGFP or EGFP-Sec6-expressing U2OS mammalian cell lysates, probed for the respective proteins as indicated. Scale bars: 10 µm. Data are mean±s.d. ****P<0.0001; ns, not significant.

Development (2021) 148, dev196345. doi:10.1242/dev.196345

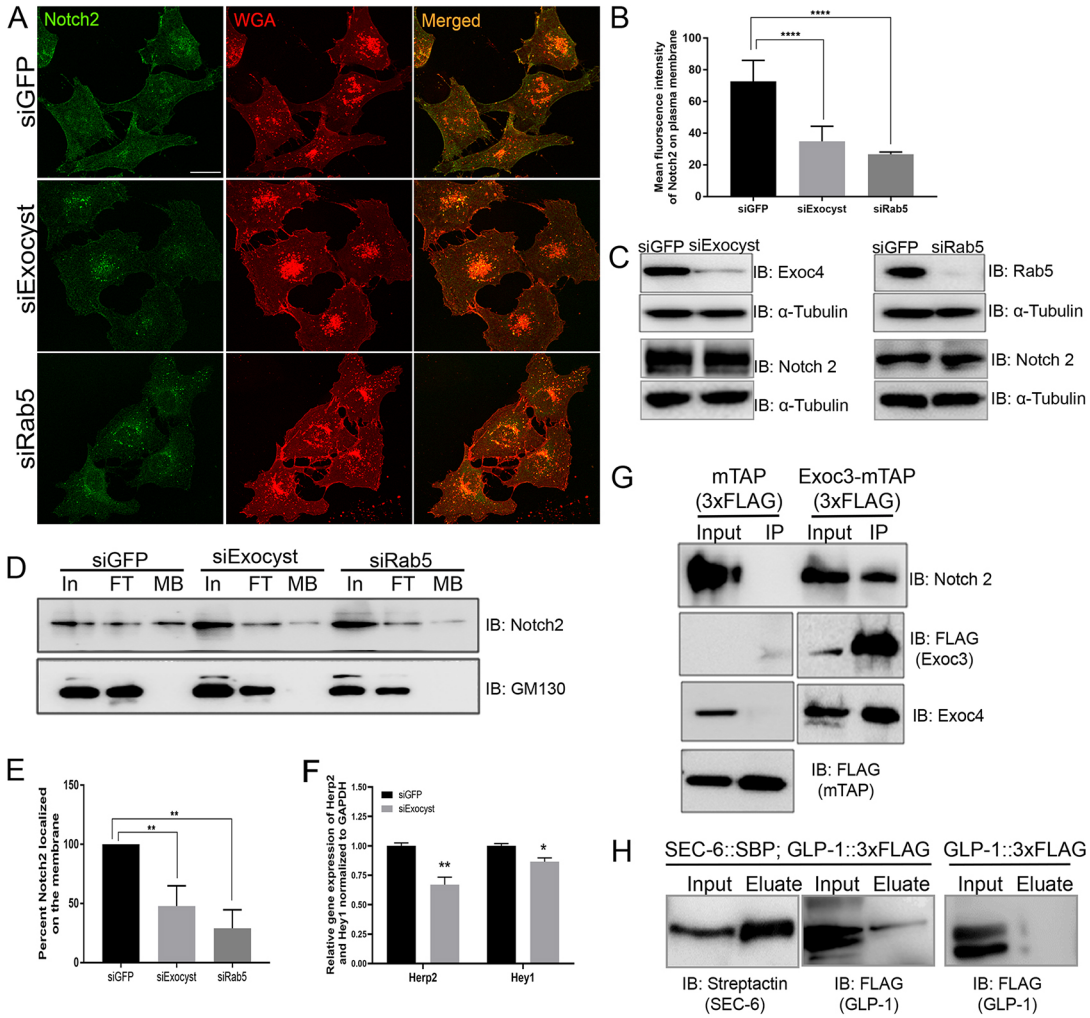

Fig. 7. The exocyst complex interacts with and traffics Notch to the plasma membrane in mammalian cells. (A) Representative confocal immunofluorescence micrographs of U2OS cells following the indicated treatment. WGA, wheat germ agglutinin, a plasma membrane marker. (B) Mean fluorescence intensity of plasma membrane-localized Notch2 after the indicated treatments from linescan image analysis; $n \geq 40$ cells, 15 or 16 cells/experiment in a minimum of three biological replicates were used for quantification. (C) Immunoblots depicting the depletion of Exoc4 and Rab5 following the indicated siRNA treatments. (D) Immunoblots for isolation of membrane-bound proteins. Input fraction (In), flow-through fraction (FT) and membrane-bound fraction (MB) probed for the indicated proteins. GM130, Golgi complex marker. (E) Densitometric quantification of immunoblot band intensities of plasma membrane-localized Notch2 from three independent biological experiments. (F) Relative expression of Herp2 and Hey1 mRNA in U2OS cells following the indicated treatments. (G) Immunoblots for FLAG immunoprecipitates from control (mTAP) or Exoc3-MTAP-expressing U2OS cell lysates and probed for the indicated proteins. (H) Immunoblots for purification of SEC-6::SBP from *C. elegans* lysates expressing SEC-6::GFP::SBP; GLP-1::GFP::3xFLAG using a Streptactin column probed with antibodies against the respective tags, showing a specific interaction of *C. elegans* SEC-6 with GLP-1. Control, worm lysates expressing only GLP-1::GFP::3xFLAG. Scale bar: 25 µm. Data are mean±s.d. *P<0.05, **P<0.01, ****P<0.0001.

membrane wheat germ agglutinin (WGA) signal as a guide, we quantified the membrane Notch levels (Fig. S7) and found them to be 20-30% decreased upon exocyst complex knockdown (Fig. 7B, Fig. S7D). We also used an orthogonal biochemical approach to exclusively purify plasma membrane-associated Notch from control and exocyst subunit-depleted cells, and measured the amount of membrane-associated Notch. The cis-Golgi matrix protein GM130 was absent from our plasma membrane fractions, confirming a clean plasma membrane preparation (Fig. 7D). We observed a significant reduction (about 40%) in the plasma membrane-expressed Notch upon exocyst subunit knockdown when compared with control siRNA treatment (Fig. 7D,E), with no change observed in the overall Notch protein levels (Fig. 7C), indicating Notch mislocalization specifically from the cell membrane. To confirm a functional effect of exocyst complex knockdown on Notch signaling in mammalian cells, we examined the mRNA expression of direct targets of Notch signaling, Hey1 and Herp2 (Iso et al., 2001), the mRNA levels of which were significantly reduced upon exocyst subunit knockdown when compared with control siRNA treatment (Fig. 7F). These results indicated that the exocyst complex regulates Notch trafficking and Notch signaling in mammalian cells. Using both approaches described above (fluorescence intensity measurements and pull down of biotinylated plasma membrane), we observed that Rab5 knockdown also led to significant reduction of Notch2 from the plasma membrane (Fig. 7A,B,D,E) as seen in our studies from *C. elegans*, without affecting total Notch protein levels (Fig. 7C), indicating a redistribution of Notch from the membrane to the cytoplasm.

Given the well-documented role of the exocyst complex in trafficking several membrane receptors to the cell surface (Fogelgren et al., 2014; Inoue et al., 2003; Langevin et al., 2005; Mao et al., 2019), we tested for a biochemical interaction between Notch and the exocyst complex by expressing a tandem affinity

Development (2021) 148, dev196345. doi:10.1242/dev.196345

purification (TAP)-tagged Exoc3 construct (Kumar et al., 2019) in U2OS cells. We observed that Notch2 specifically interacted with Exoc3 only in the test lysates and not in the control (cells expressing the MTAP-tag alone) (Fig. 7G). We also tested this interaction in *C. elegans* by generating a double transgenic strain expressing SEC-6::GFP::SBP and GLP-1::GFP::3xFLAG, and affinity purifying SEC-6 using the SBP-tag. The SBP affinity eluates showed the presence of GLP-1 in these lysates but not in worm lysates carrying only GLP-1::GFP::3×FLAG, indicating the specificity of the interaction with SEC-6 (Fig. 7H). To the best of our knowledge, this is the first report of a biochemical interaction between the Notch receptor and the exocyst complex in any animal or cell system. Collectively, these results suggest a conserved function for the exocyst complex in regulating Notch trafficking to the plasma membrane, and uncover a novel biochemical interaction between the exocyst complex and Notch in both *C. elegans* and mammalian cells.

DISCUSSION

The exocyst complex was first discovered in yeast for its role in exocytosis and has since been implicated as one of the most important regulators of polarized plasma membrane-directed vesicular fusion of Golgi-derived secretory vesicles and recycling endosomes by associating with the Rab GTPases Rab8, Rab10 and Rab11 (Das and Guo, 2011; Heider and Munson, 2012; Wu and Guo, 2015). The complex also engages with the endocytic pathway (Boehm et al., 2017; Jose et al., 2015; Kumar et al., 2019; Sommer et al., 2005). This study reports a novel role of the exocyst complex in germline stem cell (GSC) proliferation in a germline autonomous manner, likely by maintaining optimal Notch receptor levels on the GSC surface. To our knowledge, this is the first report implicating the function of the exocyst complex in stem cells in any organism.

In *C. elegans*, stem cell proliferation is mediated by the evolutionarily conserved Notch (GLP-1)-Delta (LAG-2) signaling pathway, which regulates several cell fate decisions during development and is often implicated in tumorigenesis (Gridley, 2003; Siebel and Lendahl, 2017). We found that the exocyst complex is required for regulating GSC proliferation by positively regulating Notch signaling in the GSCs, as inferred by the epistatic analysis with the loss- and gain-of-function Notch mutants (Fig. 3A-D). Importantly, RNAi of the exocyst complex resulted in downregulation of direct GSC Notch targets LST-1 and SYGL-1, and conversely the upregulation of a Notch-repressed differentiation gene GLD-1 (Fig. 3C,E,F). All of these results indicated that the exocyst complex is required for positively regulating Notch signaling in the GSCs.

We observed that exocyst complex members are expressed in the germline from GSCs to gametes (Fig. 2C, Fig. S3). The literature documents expression of the exocyst complex in embryos and in the DTC (Armenti et al., 2014; Linden et al., 2017). Reduction in the DTC plexus alone can lead to GSC proliferation defects. However, examination of the earlier reported DTC cell-autonomous function of the exocyst complex in GSC proliferation revealed a mild phenotype (12% reduction) when compared with systemic RNAi (39%) (Linden et al., 2017). We too observed the expression of SEC-6::GFP in the DTC (Fig. 2E). However, our analysis of exocyst complex function using mutant backgrounds that either enable (*rrf-1* and *sun-1::rde-1*) or disable (*ppw-1*) RNAi in the germline revealed the requirement of the exocyst complex in both the germline and the soma for GSC proliferation (Fig. 2F,G). In a broader context, the exocyst complex may be required for stem cell proliferation and differentiation in multiple systems, by trafficking key membrane proteins in both stem cells and their somatic niche cells (Jafar-Nejad et al., 2005; Mao et al., 2019), a postulate that merits further investigation.

We report a novel and strikingly asymmetric localization of Notch in GSCs through all stages of larval development and adulthood (Fig. 5A-C), with higher levels on the inner membrane when compared with the niche-facing outer membrane. Notch signaling is highly dependent on ligand-receptor stoichiometry, and therefore on receptor surface density (Andersson et al., 2011; Artavanis-Tsakonas et al., 1999), achieved by the regulated trafficking of Notch receptors to the signaling surface. Abnormal membrane receptor levels would lead either to uncontrolled proliferation or to depletion of the stem cell pool. The effect of exocyst RNAi on Notch trafficking in GSCs was similar to the defects seen with *rab-5* or *rab-11* knockdown (Fig. 5D), namely loss from the signaling interface and redistribution to the cytoplasm (Fig. 5D,E). These results together suggest defects in plasma membrane fusion of Notch-containing cellular endocytic recycling vesicles. Nevertheless, we cannot rule out the possible contribution of exocyst complex-mediated, Notch-containing post-Golgi vesicular trafficking to the plasma membrane.

Interestingly, we observed that only the aPar complex (PAR-6/PAR-3), but not the posterior Par complex (PAR-2), was required for GLP-1 trafficking to the GSC outer membrane (Fig. 6A,B). Knockdown of *par-6* also led to loss of SEC-6::GFP and accumulation of RAB-11::GFP underneath the GSC outer membrane (Fig. 6C-F). This is the first study elucidating a role of the aPar complex in modulating the exocyst complex in stem cells by impacting membrane Notch levels. Our results are supported by other studies demonstrating that the aPar proteins regulate exocyst complex-mediated trafficking in mammalian cells (Ahmed and Macara, 2017; Bryant et al., 2010; Das et al., 2014; Rosse et al., 2009), and in the *C. elegans* embryo and excretory canal (Armenti et al., 2014). Interestingly, our interactomic studies, both by mass spectrometric and yeast 2-hybrid analyses (Fig. S8), show that SEC-6 interacts with PAR-5, a known regulator of the aPar complex protein PAR-3 (Benton and St Johnston, 2003; Goldstein and Macara, 2007). We were also able to confirm the Sec6 (Exoc3)-Par5 (14-3-3ζ) interaction in mammalian cells (Fig. 6G). Taken together, these results provide novel insight into a likely mechanism through which the Par polarity complex could regulate membrane Notch levels through the exocyst complex.

Our results from mammalian cells suggest the conservation of exocyst complex-mediated, membrane-directed Notch trafficking (Fig. 7), especially due to the biochemical interaction between Notch and Exoc3/Sec6. The exocyst complex is well known to engage with post-Golgi secretory vesicles, recycling endosomes and, more recently, early endosomes by interacting with the cognate Rab GTPase markers, and is required for the fusion of these vesicles to designated sites on the plasma membrane. We envision a model of Notch trafficking wherein, upon endocytosis of Notch-positive plasma membrane through a Rab5-mediated pathway, Notch-carrying endosomes are recognized by the exocyst complex via its interaction with either or both Notch and Rab5. These vesicles could be redirected to the sorting endosomes and the recycling pathway through the interaction of the exocyst complex with Rab11-positive recycling endosomes, which could eventually fuse with the plasma membrane to deposit Notch (Fig. S9). The Notch receptor is an important addition to the increasing list of plasma membrane proteins that are trafficked to the cell surface in an exocyst-dependent manner (Fogelgren et al., 2014; Inoue et al., 2003; Langevin et al., 2005; Mao et al., 2019). In the future, a detailed characterization of the Notch-exocyst interaction would reveal the

Development (2021) 148, dev196345. doi:10.1242/dev.196345

molecular mechanistic determinants of exocyst-mediated Notch trafficking. Further studies are required to illuminate the developmentally regulated extracellular signals that could modulate exocyst complex function to eventually regulate Notch-mediated proliferation of germline stem cells.

MATERIALS AND METHODS

C. elegans strains and animal husbandry

All *C. elegans* strains used in this study are listed in Table S1 and were cultured using standard methods (Brenner, 1974). The Bristol N2 strain was used as the wild type. All transgenic strains were cultured at 25°C. Double transgenic strains were generated using standard genetic techniques. EV343 was outcrossed three times and was superficially like wild type in germline morphology, lifespan and brood count (data not shown). Several strains were sourced either from Caenorhabditis Genetics Center (CGC), USA or the National Bioresource Project (NBRP), Japan. Mutants for *sec-6* (tm4536/min1), *sec-8* (VC2648), *sec-5* (DV2689) and *sec-3* (VC2003 and VC2836) were outcrossed four times and the mutation was detected using primers listed in Table S2.

RNA interference (RNAi)

RNAi constructs for *sec-6* and *sec-8* were used from a previous study (Kumar et al., 2019). We generated the RNAi constructs for *sec-5* and *sec-3* by cloning 500 bp of the respective cDNA sequences (oligos to amplify the sequences given in Table S2) in the RNAi vector pSV2 (a gift from Dr K. Subramaniam, Indian Institute of Technology Madras, Chennai, India) at the HindIII site. The RNAi constructs for *par-6*, *par-3*, *par-2*, *rab-5* and L4440 (control vector) were sourced from the Ahringer RNAi library (a gift from Dr K. Subramaniam), and *par-5*, *rab-10*, *rab-11.1* and *rab-11.2* from the ORF RNAi library (a gift from Dr Arnab Mukhopadhyay, National Institute of Immunology, New Delhi, India). RNAi was performed as published (Timmons and Fire, 1998), except that the induced culture was concentrated 10-fold before spotting the RNAi plates and used fresh for feeding. For *sec-6* and *sec-8*, *sec-5* and *sec-3*, the L4 stage was used for feeding on the RNAi plate and F1 progeny were examined. For RNAi of *rab-5*, *rab-11* and *rab-10*, a mix of L1-L2 stage worms was placed on the plate and examined in the same generation at adulthood. For RNAi of *par-6*, *par-3*, *par-2* and *par-5*, embryos were collected on the RNAi plate and examined as they grew to adulthood.

Auxin-inducible degradation (AID) system

Construction of transgene

MVS11 {sec-6 (SMYL05[sec-6::degron::linker::GFP::SBP] II} was generated using the services of InVivo Biosystems (formerly Nemametrix and Knudra Transgenics). The degron and a linker sequence were inserted in between sec-6 and the GFP-tag in MVS01 {sec-6 (SMYL04[sec-6::GFP::SBP] II} using the CRISPR-SDM method. Briefly, two sgRNAs (sgRNA1: AGTATGTTAAAAAGAGACGC and sgRNA2: TCAGGAGCATCGATGAGTAA) were used to guide the CAS9-induced cuts and a donor-homology oligonucleotide coding for degron::linker (TGCATCAGGATCTACATCTGGATCAATGCCTAAAGATCCAGCCAAACCTCCGGCCAAGGCACAAGTTGTGGGATGGCCACCGGTGAGATCATACCGGAAGAACGTGATGGTTTCCTGCCAAAAATCAAGCGGTGGCCCGGAGGCGGCGGCGTTCGTGAAGGGGGGGACCGGATCCGGGTCCTCGACGTCGATGTC) was used to guide the repair of the cut DNA. The sgRNA-CAS9 mRNP complex was prepared prior to microinjection and was injected in *C. elegans* gonads along with the donor homology oligonucleotide and a co-CRISPR selection marker (dpy-10). Injections were performed in three sets of ten animals each. F1 progeny were screened for the co-CRISPR marker and then analyzed by PCR and sequencing for the insertion. The positive animals were made homozygous for the insertion and then out-crossed twice with the wild-type strain.

Auxin treatment

Auxin treatment was used for germline-specific degradation of SEC-6 by combining MVS03 with a germline-expressed TIR1 (CA1199 – sun1p::TIR1::mRuby::sun-1 3′UTR). For auxin treatment, the NNGM plates were supplemented with 2 mM Indole 3-acetic acid (IAA/auxin). OP50 grown in 4×YPD media was concentrated five times before seeding and growing for 12 h. The double transgenic worms were exposed to auxin from early L4 stage, placed on the plates and incubated at 25°C. Regular NNGM plates were used as controls. Animals were examined 48 h post-auxin treatment for GSC proliferation defects. Worm lysates from each pool of treatment were analyzed by western blots using an antibody against SBP to determine the efficiency of degradation.

Immunostaining

Gonads were dissected from worms using standard procedures (Ariz et al., 2009) and fixed in 4% formaldehyde for 30 min at room temperature for anti-phospho histone 3 (PH3) and anti-V5 staining, or for 10 min for anti-WAPL-1 staining. The fixative was washed twice with PBS-Tween (phosphate-buffered saline pH 7.4 containing 0.1% Tween 20) followed by successive incubations for 5 min in methanol at −20°C and 10 min in acetone at −20°C. Worms were washed twice in PBS-Tween and blocked with blocking buffer (PBS+5% BSA+0.1% Tween20) for 1 h. Primary antibodies (anti-PH3 antibody, Thermo Scientific, PA5-17869; anti-V5, BioRad, MCA1360GA; anti-WAPL-1, Novus Biologicals, 49300002) were used at 1:1000 dilution and incubated at 4°C overnight. Alexafluor 488-conjugated anti-rabbit secondary antibody (Jackson ImmunoResearch) was used at 1:10,000 dilution and DAPI at a final concentration of 25 ng/µl. Finally, the gonads were mounted in Prolong Gold mounting medium (Invitrogen). For only DAPI staining, worms were dissected and fixed in 4% formaldehyde (with 0.1 M phosphate buffer) for 1 h at room temperature and subsequently washed twice in PBS-Tween. Gonads were incubated in chilled methanol for 5 min at −20°C, washed twice in PBS-Tween and finally stained with DAPI solution for 5 min. Excess stain was washed off twice with PBS-Tween and the gonads mounted in Prolong Gold mounting medium. Alternatively, whole worms were fixed in 100% chilled methanol at room temperature for 1 h and processed similarly as carried out for formaldehyde-fixed gonads.

Microscopy and image preparation

To examine fluorescence in live worms, either the whole worm or the dissected gonad was mounted in 2 mM levamizole solution (Sigma) on 2% agar pads. For immunostaining, gonads were mounted in Prolong Gold mounting medium on 2% agar pads. All fluorescence images were acquired using a Leica point scanning laser confocal microscope (TCS SP5 II or TCS SP8) and the images were processed using the LASX software (Leica Microsystems). Images were finally assembled using Adobe Photoshop PS5. Whole-mount worm images and gonads were imaged in overlapping frames, and merged together using the photomerge tool of PS5. All images of a specific panel were processed similarly using brightness/contrast or the levels filter of Photoshop. The Clone stamp tool was used to erase the carcass debris or the neighboring worms/gonads by cloning the neighboring blank region of the image that did not specifically represent any productive image.

Quantification and statistical analysis

Quantitation of GLP-1::GFP using EV343; OD70

Hand-drawn line scan profiles in the LASX software (Leica Microsystems) were used to quantitate the mean fluorescence intensity of GLP-1::GFP from the single focal plane that best showed the outer and inner membranes of several germline stem cells in the best focus, using a membrane marker (PH::mCherry) as the reference for membrane. About 8-10 cells per gonad and a minimum of 12-15 gonads were used for quantitation per experiment for a minimum of three independent biological repeats.

Integrated fluorescence density measurement for GLD-1::GFP, LST-1::V5 and SYGL-1::V5

We used the Image J software to calculate the integrated fluorescence density of GLD-1::GFP in the control and the *sec-6* and *sec-8* RNAi gonads. Rectangular ROIs were drawn in the area of protein expression and the integrated fluorescence density calculated. These values were corrected for background subtraction by drawing an equal-sized ROI outside the gonad in

Development (2021) 148, dev196345. doi:10.1242/dev.196345

the unstained region. For GLD-1::GFP, ROIs were drawn in the first 10-gcd (germ cell diameters) region using the maximum projection image of a particular gonad. A minimum of 8-10 gonads were used per experiment for a minimum of three independent biological repeats.

Notch2 levels on the mammalian cell surface

Notch2 fluorescence intensities at the plasma membrane were quantified using the LASX software from Leica. A line was drawn across the plasma membrane extending up to 10-20 pixels inside the cell from the cortex. Wheat Germ Agglutinin (WGA)-594 was used to label the plasma membrane and Notch2 intensity peaks coinciding with the WGA peak were recorded. A minimum of five and up to ten regions of interest (ROI) per cell from five cells per field were used. In every field, a total of 40-50 ROIs were drawn and a total of 12-15 cells per experiment were analyzed for each experimental condition. Data from a minimum of three biological repeats was used to arrive at the final average. A two-tailed, unpaired Student's *t*-test was used to calculate the statistical significance between the control and the test samples. To calculate the cortex versus cytoplasm ratio of Notch2 receptor, we measured the membrane levels of Notch2 using line scans that overlapped with WGA staining at or near the membrane as described above, and fractionated it with Notch intensity at 10 nm below the cortex as described by Sharma et al. (2020).

SEC-6::GFP near the membrane

To calculate the amount of SEC-6::GFP underneath the plasma membrane, we drew line scans using LASX software (Leica Microsystems) across the cell membrane spanning from the nuclei of one cell to the other in the progenitor zone, keeping red fluorescence from PH::mCherry as the guide for the plasma membrane. The peak fluorescence intensity around the plasma membrane was noted for each line scan. We drew a total of two linescans per cell and used 10 cells per gonad for these calculations. In each experiment, about 10 gonads were used for the calculation.

RAB-11::GFP on the membrane

To measure the accumulation of RAB-11::GFP on the plasma membrane of the germ cells in the PZ, we used linescans using the LASX software (Leica Microsystems) to calculate the mean fluorescence intensity of GFP at the plasma membrane. 10 cells per gonad and 10-12 gonads in each experiment were used for these measurements.

Total cell count in the progenitor zone (PZ)

The total number of germ cells in the PZ was calculated using the Imaris software suite 8.4.1 (Bitplane) for image analysis as mentioned in Gopal et al. (2017). The gonads were first cropped to display only the progenitor zone as far as the first layer of the transition zone (TZ). The average size of the nuclei was estimated by measuring the size of five nuclei randomly for the given gonad. Such images were subjected to cell quantitation using the spots tool of the software. Nuclear diameter was provided as 2-3 µm depending upon the measurements made earlier. The surface was created using the automatic wizard of the software to pick all nuclei of the given size. Finally, any acellular DAPI-spots outside the gonad or coming from any neighboring gonad were eliminated using the deselection tool.

Length of the progenitor zone (PZ)

The different stages of germ cells can be easily recognized based on their different nuclear morphology (Hirsh et al., 1976; Hubbard and Greenstein; Pazdernik and Schedl, 2013). The GSCs present in close contact with the niche cell (extreme left of the images) show floret-shaped nuclei (Fig. 1J, DAPI inset). As the cells move away from the niche and start transitioning into the meiotic program, the nuclei become crescent-shaped (thought to be due to chromosome pairing). Further on, the nuclei in the pachytene zone (meiotic zone) have a distinct noodle-shaped morphology. A single confocal plane of the middle section of dissected hermaphrodite gonads stained with DNA-binding dye (DAPI) was used to count the number of germ cell nuclei present in a single row of the gonad from the distal end to the first layer of transition zone (TZ) displaying multiple crescent-shaped nuclei. A minimum of 15 gonads (one gonad/worm) was used for this analysis. Any twisted or broken gonads were not used for this analysis. The result was reported as the number of germ cell diameters (GCDs) in the progenitor zone per gonad.

Mitotic index

The ratio of PH3-positive cells to the total number of cells in the progenitor zone was calculated from dissected hermaphrodite gonads of the respective genotype stained with an anti-PH3 antibody and the DNA-binding dye (DAPI). The total number of PH3-positive cells was manually counted in all the *z*-sections. The total number of germ cells in the progenitor zone (PZ) was calculated using the IMARIS software suite, as mentioned above.

Statistical analysis

Data from three or four experiments were used to calculate the average and the standard deviation. An unpaired Student's *t*-test with Welch's correction was used to calculate the statistical significance between the control and test samples using the Graph Pad Prism software (*P<0.05, **P<0.01, ***P<0.001 and ****P<0.0001).

Yeast two-hybrid screen

Yeast two-hybrid screening was performed by Hybrigenics Services (http://www.hybrigenics-services.com). Full-length SEC-6 (NCBI reference NM_062605.7) was PCR amplified and cloned into pB27 (derived from pBTM116) as a C-terminal fusion to LexA (LexA-sec-6). The construct was confirmed by sequencing the entire insert and used as a bait to screen a random-primed *C. elegans* mixed stages cDNA library constructed into the pP6 (derived from pGADGH) plasmid. A total of 98 million clones (10-fold the complexity of the library) were screened using a mating approach with YHGX13 (Y187 ade2-101::loxP-kanMX-loxP, matα) and L40ΔGal4 (mata) yeast strains as previously described (Fromont-Racine et al., 1997). Finally, 254 His+ colonies were selected on a medium lacking tryptophan, leucine and histidine, and supplemented with 0.5 mM 3-aminotriazole to handle bait autoactivation. The prey fragments of the positive clones were amplified by PCR and sequenced at their 5′ and 3′ junctions for identification using a fully automated procedure. A confidence score (PBS, for Predicted Biological Score) was attributed to each interaction as previously described (Formstecher et al., 2005).

Purification of SEC-6::GFP::SBP using a streptactin column

Worms expressing SEC-6 tagged with GFP and SBP were cultured on a large scale in a synchronized manner (Chan et al., 2014). About 3-5 ml (packed volume) of worms were collected and suspended in lysis buffer [50 mm HEPES-KOH (pH 7.6), 150 mm KCl, 1 mM EDTA, 0.5% Nonidet P-40 and 10% glycerol] containing the protease inhibitor mix from Sigma (P8340). The resulting slurry was suspended frozen in liquid nitrogen. The worm lysates were prepared by crushing the frozen pellet in liquid nitrogen bath according to Chan et al. (2014). For protein purification, a 1 ml streptactin column (GE) was used. The column was washed with 10 volumes of deionized water and then equilibrated with five volumes of lysis buffer. The prepared worm lysate was passed through the equilibrated streptactin column. Bound proteins were washed with 10 volumes of wash buffer [50 mm HEPES-KOH (pH 7.6), 150 mM KCl, 1 mM EDTA, 0.2% Nonidet P-40 and 4% glycerol]. Fractions of input, flowthrough and washes were collected for later analysis. Finally, the bound proteins were eluted using five volumes of elution buffer containing desthio-biotin [50 mm HEPES-KOH (pH 7.6), 150 mm KCl, 1 mm EDTA and 2.5 mM desthio-biotin]. The resulting eluate was concentrated using Amicon Ultra Centrifugal Filters (3 kDa cut-off) to a final volume of 150 µl. The concentrated eluate was mixed with 4×SDS sample loading buffer (Laemmli buffer) and subjected to western blot analysis along with input, flow through and wash fractions collected earlier.

Liquid chromatography (LC)/mass spectrometry (MS) analysis

Worm lysate expressing SEC-6::GFP::SBP was used to purify interacting partners of SEC-6 using the streptactin column as mentioned above. The eluate was concentrated using Amicon Ultra Centrifugal Filters (3 kD cut-off) to a final volume of 150 µl and suspended in 4×SDS sample loading buffer. 120 µl of the eluate was loaded onto the SDS-PAGE gel and the rest

Development (2021) 148, dev196345. doi:10.1242/dev.196345

was saved for western blotting analysis to confirm the pull down. The gel was run until the highest molecular weight band entered the separating gel and was then stained with Coomassie Brilliant Blue (CBB) using standard protocols. The lane carrying the sample was cut into 1 mm^2 pieces, which were first destained and washed using different dilutions of acetonitrile prepared in sodium bicarbonate, then reduced using 5 mM dithiothreitol (DTT) and finally alkylated using 20 mM oodoacetamide. The gel pieces were washed and again dehydrated using 100% acetonitrile. In-gel trypsin digestion was carried out using mass spectrometry grade Trypsin Gold (Promega) at a final concentration of 10 ng/µl for 16 h at 37°C. Post-digestion, the peptides were extracted using 60% acetonitrile solution followed by 100% acetonitrile by gentle sonicating for 15 min at each step. The resulting supernatant containing digested peptides was vacuum-dried at 42°C. Finally, the peptides were desalted using ZipTips containing C18 resin before subjecting to electrospray ionization LC/MS analysis (ABSciex 5600). The resulting data were analyzed against the *C. elegans* protein database using both Paragon and Mascot algorithms to identify the bound proteins. The proteins identified in the control sample were subtracted from the test using Venny 2.1.0 to arrive at the final list of potential interacting partners.

RNA isolation, cDNA synthesis and quantitative RT-PCR analysis

RNA isolation and cDNA synthesis

About 100 worms were placed in 100 µl of Tri-reagent (Sigma) and stored at −80°C. The worm suspension in Tri-reagent was subjected to three or four cycles of freeze and thaw. After that worms were crushed using a pestle in 1.5 ml centrifuge tube. RNA was isolated according to the manufacturer's protocol. The RNA was subjected to DNase I (Fermentas) treatment for 15 min according to the manufacturer's protocol. DNase was heat-killed at 70°C for 10 min, and RNA was extracted with phenol-chloroform and precipitated. The final RNA pellet was dissolved in 11.5 µl of RNase-free water and measured for quality and quantity. Total RNA (~1-2 µg) was used for reverse transcription. Reverse transcription was carried out using MuMLV-Reverse Transcriptase (Fermentas) according to the manufacturer's protocol using oligo-dT. The final cDNA was made up to 100 µl by adding TE (pH 8.0). For mammalian cells, cells from a single 35 mm dish 48 h post siRNA treatment were harvested and suspended in Tri reagent.

Quantitative RT-PCR analysis

RT-qPCR was performed using a 7500 Fast real time PCR system (Applied Biosystems/Life Technologies). 100 ng cDNA per reaction was used for both test and control, and the reaction was performed in triplicate for each primer pair using SYBR Premix Ex Taq II reagents (TaKaRa). PCR conditions used were: initial denaturation at 95°C (2 min), cycling stage denaturation at 95°C (5 s), and annealing and extension at 60°C (30 s) for a total of 40 cycles. The cycle threshold (Ct) value was normalized to actin Ct values and an average from three independent biological replicates from control and test were plotted as a graph.

Mammalian cell culture

Cell culture, plasmid and siRNA transfection and imaging

U2OS cells (a gift from Stephen J. Doxsey, University of Massachusetts Medical School, Worcester, USA) were grown and maintained in high-glucose DMEM supplemented with penicillin and streptomycin. Both cell lines were cultured at 37°C, 5% carbon dioxide and 95% humidity. Cells were transfected with plasmid construct (Exoc3-mTAP) using Xtremgene HP (Roche) or siRNAs (against the exocyst complex members and Rab5 as indicated through western blots) using Dharmafect 1 (Dharmacon) and assayed 48 h after transfection. siRNAs used for exocyst members were same as used by Neto et al. (2013a,b) and for Rab5 were the same as used by Chen et al. (2009). For fixed cell imaging, coverslips were imaged at 63× on a Leica TCS SP8 laser scanning confocal microscope using the confocal mode.

Antibodies, DNA and reagents

Anti Notch2 antibody was purchased from Cell Signaling Technologies and used as described previously (Li et al., 2015) (5732; 1:1000 for western blotting and 1:200 for immunofluorescence assay). Primary antibodies directed against exocyst subunits were used as described previously (Neto et al., 2013a,b). Anti Exoc3 (Sec6) was from Thermo Scientific (MA1-2548; dilution 1:200 for western blotting), Exoc4 (Sec8) was from Abcam (ab13254; dilution 1:1000 for western blotting) and Exoc2 (Sec5) was from Proteintech 12751-1-AP; dilution 1:1500). Anti-FLAG M2 and anti α-tubulin antibodies were from Sigma (FLAG-M2: F-1804 and dilution 1:10,000 for western blotting; tubulin: T6199 and dilution 1:2000 for western blotting). Anti-Rab5 antibody was from Abcam (ab199530; dilution 1:1000 for western blotting) and was used as described previously (Chen et al., 2014a). Anti-GAPDH antibody was from Thermo Scientific (AM4300; dilution 1:500 for western blotting). Anti-GM130 antibody was from Abcam (ab52649; dilution 1:2000 for western blotting). Anti-mouse and anti-rabbit Alexa-488-conjugated secondary antibodies (715-545-150 and 711-545-152), and anti-mouse, anti-rabbit Alexa-594-conjugated secondary antibodies (715-585-150 and 711-585-152) for immunofluorescence were purchased from Jackson Immunoresearch. Horseradish peroxidase (HRP)-conjugated anti-mouse (715-035-150) and anti-rabbit (711-035-152) secondary antibodies for western blot analysis were purchased from Jackson Immunoresearch. Exoc3 cDNA was amplified from a human cDNA library and cloned in the pmTAP-mVenus vector (a kind gift from Dannel McCollum, University of Massachusetts Medical School, Worcester, USA) using Hind III (forward primer, 5′ CCT AAG CTT ATG AAG GAG ACA GAC CGG GAG G3′) and Not I (reverse primer, 5′GCG GCC GCT CTT GAG CAG CTT GGC CAC GTT C3′) restriction sites and sequenced.

Immunofluorescence

Cells were seeded on glass coverslips 24 h prior to siRNA or plasmid transfection. 48 h post transfection, media were removed and the cells were washed twice with 1× phosphate-buffered saline (PBS) and fixed in methanol at −20°C for 30 min. Cells were washed thrice with 1× PBS and rehydrated by incubating in 1× PBS for another 30 min, blocked for 1 h at room temperature with 1% BSA and 22.52 mg/ml glycine in PBST (PBS+ 0.1% Tween 20). Primary (anti-Notch2 antibody) and secondary antibodies were diluted in 1% BSA in PBST. Primary antibody incubation was carried out overnight at 4°C. After primary antibody incubation, coverslips were washed twice with 1× PBS only. Secondary antibody incubation was performed for 1 h at room temperature and similar washing steps were performed. Coverslips were mounted in Prolong Gold/Prolong Diamond anti-fade mounting reagent containing DAPI (Thermo Scientific) and allowed to dry and set overnight in the dark.

Immunoprecipitation

U2OS cells were transfected with the Exoc3-mTAP construct. 48 h after transfection, cells were lysed in immunoprecipitation (IP) buffer containing 50 mM HEPES, 150 mM NaCl, 0.1% NP-40 supplemented with HALT protease and phosphatase inhibitor cocktail (Thermo Scientific). All steps from lysis onwards were performed on ice. Cells were briefly sonicated for 50 s at 50% amplitude in five pulses and centrifuged at 15,000 ***g*** (12,000 rpm) at 4°C for 30 min. The supernatant thus obtained (input) was stored on ice. FLAG M2 affinity gel (Sigma-Aldrich) was washed thrice in the same IP buffer. 2 mg of input (total protein) was taken for IP and incubated with the affinity gel overnight in a cold room on a nutator with gentle rotation. Following incubation, the sample was centrifuged at 200 ***g*** for 10 min, the unbound supernatant decanted and the bound affinity gel washed thrice in IP buffer. The bound protein was eluted by boiling the affinity gel in 2× Laemmli buffer at 95°C for 10 min and the samples were probed by western blotting.

Cell surface biotinylation and pulldown

Plasma membrane biotinylation of U2OS cells was performed as described previously (Phillips-Krawczak et al., 2015). Equal amounts of cell lysates from both control and siRNA-treated cells were incubated for 30 min at 4°C with Sulfo-NHS-SS-biotin (as part of the Cell Surface Isolation kit, Thermo Scientific, 89881) dissolved in 1× PBS for biotinylation of plasma membrane proteins. Biotinylated membranes were affinity precipitated down using NeutrAvidin agarose resin from the same kit and eluted in

2× Laemmli buffer with 50 mM DTT and probed for the indicated proteins by western blotting.

Western blotting and densitometry

Samples for western blotting were lysed in 2× Laemmli buffer and the protein concentration was estimated by the Bradford assay method using the CB-X protein assay kit (G-Biosciences, 786-894). For ascertaining siRNA-mediated knock-down, 20 µg of cell lysates were loaded on a 10% SDS-PAGE gel and electrophoresis was performed before transferring the resolved proteins onto Immobilon-P PVDF membrane (Millipore). Blocking of the membrane was performed in 1× TBST containing 5% BSA (Sigma-Aldrich) followed by overnight incubation in the primary antibody at 4°C. Membranes were washed with 1× TBST for 2 h and incubated with HRP-conjugated secondary antibody for 1 h at room temperature. Blots were washed with 1× TBST for 3 h and ECL substrate (Luminata Forte, Millipore) was added to develop signal. Blot images were captured in an Image Quant LAS 4000 series (GE Healthcare Life Sciences). Western blots from three independent experiments were quantified for probed proteins through densitometric analyses using ImageQuant TL software (GE Healthcare Life Sciences) for graphical representation.

Acknowledgements

We thank Prof. K Subramaniam (Indian Institute of Technology Madras) for *C. elegans* strains, RNAi constructs, pSV2 and L4440 vectors, for *E. coli* strains OP50, NA22 and HT115, and for critical comments during the study. We thank Dr Arnab Mukhopadhyay (National Institute of Immunology, New Delhi, India) for initial help with *C. elegans* infrastructure, and a few RNAi constructs, and Prof. Judith Kimble and Dr Sarah Crittenden (University of Wisconsin-Madison, USA) for the strain JK5933. We thank Prof. Stephen J Doxsey for U2OS cells, Prof. Dannel McCollum for the pMTAP-mVenus expression vector (both at the University of Massachusetts Medical School, Worcester, USA) and Dr Divya Chandran (Regional Centre for Biotechnology, India) for the gift of auxin. Several strains were provided by the CGC (funded by NIH Office of Research Infrastructure Programs, P40 OD010440) and NBRP (Japan). We thank WormBase for all *C. elegans*-related information. We are grateful to the Regional Centre for Biotechnology for providing the requisite infrastructure and to the members of the Laboratory of Cellular Dynamics at the Regional Centre for Biotechnology for critical comments and suggestions during the study.

Competing interests

The authors declare no competing or financial interests.

Author contributions

Conceptualization: K.P., S.V.S.M.; Methodology: K.P., S.D., H.K., D.P.; Software: K.P., S.D.; Validation: K.P., S.D., H.K., D.P., S.M.; Formal analysis: K.P., S.D., H.K., D.P.; Investigation: K.P., S.D., H.K., D.P.; Resources: S.M.; Data curation: K.P., S.D., H.K.; Writing - original draft: K.P.; Writing - review & editing: K.P., S.V.S.M.; Visualization: K.P., S.V.S.M.; Supervision: S.V.S.M.; Project administration: K.P., S.V.S.M.; Funding acquisition: K.P., S.V.S.M.

Funding

This work was supported by The Wellcome Trust DBT India Alliance fellowship (IA/E/13/1/501 to K.P.). H.K. and S.D. were supported by research fellowships from the Regional Centre for Biotechnology (Pali, India) and by funding to S.V.S.M. from the Regional Centre for Biotechnology, the Department of Biotechnology, Ministry of Science and Technology, India (BT/PR6420/GBD/27/435/2012) and the Science and Engineering Research Board (EMR/2016/007842). D.P. is supported by a student fellowship from the University Grants Commission.

Peer review history

The peer review history is available online at https://journals.biologists.com/dev/article-lookup/doi/10.1242/dev.196345

References

Ahmed, S. M. and Macara, I. G. (2017). The Par3 polarity protein is an exocyst receptor essential for mammary cell survival. *Nat. Commun.* **8**, 14867. doi:10.1038/ncomms14867

Amini, R., Goupil, E., Labella, S., Zetka, M., Maddox, A. S., Labbe, J.-C. and Chartier, N. T. (2014). C. elegans Anillin proteins regulate intercellular bridge stability and germline syncytial organization. *J. Cell Biol.* **206**, 129-143. doi:10.1083/jcb.201310117

Andersson, E. R., Sandberg, R. and Lendahl, U. (2011). Notch signaling: simplicity in design, versatility in function. *Development* **138**, 3593-3612. doi:10.1242/dev.063610

Ariz, M., Mainpal, R. and Subramaniam, K. (2009). C. elegans RNA-binding proteins PUF-8 and MEX-3 function redundantly to promote germline stem cell mitosis. *Dev. Biol.* **326**, 295-304. doi:10.1016/j.ydbio.2008.11.024

Armenti, S. T., Chan, E. and Nance, J. (2014). Polarized exocyst-mediated vesicle fusion directs intracellular lumenogenesis within the C. elegans excretory cell. *Dev. Biol.* **394**, 110-121. doi:10.1016/j.ydbio.2014.07.019

Artavanis-Tsakonas, S., Rand, M. D. and Lake, R. J. (1999). Notch signaling: cell fate control and signal integration in development. *Science* **284**, 770-776. doi:10.1126/science.284.5415.770

Austin, J. and Kimble, J. (1987). glp-1 is required in the germ line for regulation of the decision between mitosis and meiosis in C. elegans. *Cell* **51**, 589-599. doi:10.1016/0092-8674(87)90128-0

Balklava, Z., Pant, S., Fares, H. and Grant, B. D. (2007). Genome-wide analysis identifies a general requirement for polarity proteins in endocytic traffic. *Nat. Cell Biol.* **9**, 1066-1073. doi:10.1038/ncb1627

Barth, J. M. and Köhler, K. (2014). How to take autophagy and endocytosis up a notch. *Biomed. Res. Int.* **2014**, 960803. doi:10.1155/2014/960803

Benton, R. and St Johnston, D. (2003). Drosophila PAR-1 and 14-3-3 inhibit Bazooka/PAR-3 to establish complementary cortical domains in polarized cells. *Cell* **115**, 691-704. doi:10.1016/S0092-8674(03)00938-3

Boehm, C. M., Obado, S., Gadelha, C., Kaupisch, A., Manna, P. T., Gould, G. W., Munson, M., Chait, B. T., Rout, M. P. and Field, M. C. (2017). The trypanosome exocyst: a conserved structure revealing a new role in endocytosis. *PLoS Pathog.* **13**, e1006063. doi:10.1371/journal.ppat.1006063

Brenner, S. (1974). The genetics of Caenorhabditis elegans. *Genetics* **77**, 71-94. doi:10.1093/genetics/77.1.71

Brenner, J. L. and Schedl, T. (2016). Germline stem cell differentiation entails regional control of cell fate regulator GLD-1 in Caenorhabditis elegans. *Genetics* **202**, 1085-1103. doi:10.1534/genetics.115.185678

Bryant, D. M., Datta, A., Rodríguez-Fraticelli, A. E., Peränen, J., Martín-Belmonte, F. and Mostov, K. E. (2010). A molecular network for de novo generation of the apical surface and lumen. *Nat. Cell Biol.* **12**, 1035-1045. doi:10.1038/ncb2106

Chan, K. K. M., Seetharaman, A., Bagg, R., Selman, G., Zhang, Y., Kim, J. and Roy, P. J. (2014). EVA-1 functions as an UNC-40 Co-receptor to enhance attraction to the MADD-4 guidance cue in Caenorhabditis elegans. *PLoS Genet.* **10**, e1004521. doi:10.1371/journal.pgen.1004521

Chen, P.-I., Kong, C., Su, X. and Stahl, P. D. (2009). Rab5 isoforms differentially regulate the trafficking and degradation of epidermal growth factor receptors. *J. Biol. Chem.* **284**, 30328-30338. doi:10.1074/jbc.M109.034546

Chen, P.-I., Schauer, K., Kong, C., Harding, A. R., Goud, B. and Stahl, P. D. (2014a). Rab5 isoforms orchestrate a "division of labor" in the endocytic network; Rab5C modulates Rac-mediated cell motility. *PLoS ONE* **9**, e90384. doi:10.1371/journal.pone.0090384

Chen, S., Li, L., Li, J., Liu, B., Zhu, X., Zheng, L., Zhang, R. and Xu, T. (2014b). SEC-10 and RAB-10 coordinate basolateral recycling of clathrin-independent cargo through endosomal tubules in Caenorhabditis elegans. *Proc. Natl. Acad. Sci. USA* **111**, 15432-15437. doi:10.1073/pnas.1408327111

Clague, M. J. and Urbé, S. (2001). The interface of receptor trafficking and signalling. *J. Cell Sci.* **114**, 3075-3081. doi:10.1242/jcs.114.17.3075

Das, A. and Guo, W. (2011). Rabs and the exocyst in ciliogenesis, tubulogenesis and beyond. *Trends Cell Biol.* **21**, 383-386. doi:10.1016/j.tcb.2011.03.006

Das, A., Gajendra, S., Falenta, K., Oudin, M. J., Peschard, P., Feng, S., Wu, B., Marshall, C. J., Doherty, P., Guo, W. et al. (2014). RalA promotes a direct exocyst-Par6 interaction to regulate polarity in neuronal development. *J. Cell Sci.* **127**, 686-699. doi:10.1242/jcs.145037

Fogelgren, B., Zuo, X., Buonato, J. M., Vasilyev, A., Baek, J.-I., Choi, S. Y., Chacon-Heszele, M. F., Palmyre, A., Polgar, N., Drummond, I. et al. (2014). Exocyst Sec10 protects renal tubule cells from injury by EGFR/MAPK activation and effects on endocytosis. *Am. J. Physiol. Renal. Physiol.* **307**, F1334-F1341. doi:10.1152/ajprenal.00032.2014

Formstecher, E., Aresta, S., Collura, V., Hamburger, A., Meil, A., Trehin, A., Reverdy, C., Betin, V., Maire, S., Brun, C. et al. (2005). Protein interaction mapping: a Drosophila case study. *Genome Res.* **15**, 376-384. doi:10.1101/gr.2659105

Fortini, M. E. and Bilder, D. (2009). Endocytic regulation of Notch signaling. *Curr. Opin. Genet. Dev.* **19**, 323-328. doi:10.1016/j.gde.2009.04.005

Fromont-Racine, M., Rain, J.-C. and Legrain, P. (1997). Toward a functional analysis of the yeast genome through exhaustive two-hybrid screens. *Nat. Genet.* **16**, 277-282. doi:10.1038/ng0797-277

Goldstein, B. and Macara, I. G. (2007). The PAR proteins: fundamental players in animal cell polarization. *Dev. Cell* **13**, 609-622. doi:10.1016/j.devcel.2007.10.007

Gopal, S., Boag, P. and Pocock, R. (2017). Automated three-dimensional reconstruction of the Caenorhabditis elegans germline. *Dev. Biol.* **432**, 222-228. doi:10.1016/j.ydbio.2017.10.004

Grant, B. and Hirsh, D. (1999). Receptor-mediated endocytosis in the Caenorhabditis elegans oocyte. *Mol. Biol. Cell* **10**, 4311-4326. doi:10.1091/mbc.10.12.4311
Grant, B. D. and Sato, M. (2006). Intracellular trafficking (ed. The C. elegans Research Community). *WormBook* doi:10.1895/wormbook.1.77.1, http://www.wormbook.org
Green, R. A., Kao, H.-L., Audhya, A., Arur, S., Mayers, J. R., Fridolfsson, H. N., Schulman, M., Schloissnig, S., Niessen, S., Laband, K. et al. (2011). A high-resolution C. elegans essential gene network based on phenotypic profiling of a complex tissue. *Cell* **145**, 470-482. doi:10.1016/j.cell.2011.03.037
Gridley, T. (2003). Notch signaling and inherited disease syndromes. *Hum. Mol. Genet.* **12**, R9-R13. doi:10.1093/hmg/ddg052
Hanna, M., Wang, L. and Audhya, A. (2013). Worming our way in and out of the Caenorhabditis elegans germline and developing embryo. *Traffic* **14**, 471-478. doi:10.1111/tra.12044
Hansen, D., Wilson-Berry, L., Dang, T. and Schedl, T. (2004). Control of the proliferation versus meiotic development decision in the C. elegans germline through regulation of GLD-1 protein accumulation. *Development* **131**, 93-104. doi:10.1242/dev.00916
He, B. and Guo, W. (2009). The exocyst complex in polarized exocytosis. *Curr. Opin. Cell Biol.* **21**, 537-542. doi:10.1016/j.ceb.2009.04.007
Heider, M. R. and Munson, M. (2012). Exorcising the exocyst complex. *Traffic* **13**, 898-907. doi:10.1111/j.1600-0854.2012.01353.x
Hirsh, D., Oppenheim, D. and Klass, M. (1976). Development of the reproductive system of Caenorhabditis elegans. *Dev. Biol.* **49**, 200-219. doi:10.1016/0012-1606(76)90267-0
Hubbard, E. J. and Greenstein, D. (2005). Introduction to the germ line (ed. The C. elegans Research Community). *WormBook* doi:10.1895/wormbook.1.18.1, http://www.wormbook.org
Hubbard, E. J. A. and Greenstein, D. Introduction to the germ line. In *WormBook* (ed. **T. C. e. R. Community**).
Hurd, T. W., Fan, S., Liu, C.-J., Kweon, H. K., Hakansson, K. and Margolis, B. (2003). Phosphorylation-dependent binding of 14-3-3 to the polarity protein Par3 regulates cell polarity in mammalian epithelia. *Curr. Biol.* **13**, 2082-2090. doi:10.1016/j.cub.2003.11.020
Inoue, M., Chang, L., Hwang, J., Chiang, S.-H. and Saltiel, A. R. (2003). The exocyst complex is required for targeting of Glut4 to the plasma membrane by insulin. *Nature* **422**, 629-633. doi:10.1038/nature01533
Iso, T., Sartorelli, V., Chung, G., Shichinohe, T., Kedes, L. and Hamamori, Y. (2001). HERP, a new primary target of Notch regulated by ligand binding. *Mol. Cell. Biol.* **21**, 6071-6079. doi:10.1128/MCB.21.17.6071-6079.2001
Jafar-Nejad, H., Andrews, H. K., Acar, M., Bayat, V., Wirtz-Peitz, F., Mehta, S. Q., Knoblich, J. A. and Bellen, H. J. (2005). Sec15, a component of the exocyst, promotes notch signaling during the asymmetric division of Drosophila sensory organ precursors. *Dev. Cell* **9**, 351-363. doi:10.1016/j.devcel.2005.06.010
Jantsch-Plunger, V. and Glotzer, M. (1999). Depletion of syntaxins in the early Caenorhabditis elegans embryo reveals a role for membrane fusion events in cytokinesis. *Curr. Biol.* **9**, 738-745. doi:10.1016/S0960-9822(99)80333-9
Jiu, Y., Jin, C., Liu, Y., Holmberg, C. I. and Jäntti, J. (2012). Exocyst subunits Exo70 and Exo84 cooperate with small GTPases to regulate behavior and endocytic trafficking in C. elegans. *PLoS ONE* **7**, e32077. doi:10.1371/journal.pone.0032077
Jiu, Y., Hasygar, K., Tang, L., Liu, Y., Holmberg, C. I., Bürglin, T. R., Hietakangas, V. and Jäntti, J. (2014). par-1, atypical pkc, and PP2A/B55 sur-6 are implicated in the regulation of exocyst-mediated membrane trafficking in Caenorhabditis elegans. *G3 (Bethesda)* **4**, 173-183. doi:10.1534/g3.113.006718
Jose, M., Tollis, S., Nair, D., Mitteau, R., Velours, C., Massoni-Laporte, A., Royou, A., Sibarita, J.-B. and McCusker, D. (2015). A quantitative imaging-based screen reveals the exocyst as a network hub connecting endocytosis and exocytosis. *Mol. Biol. Cell* **26**, 2519-2534. doi:10.1091/mbc.E14-11-1527
Kadyk, L. C. and Kimble, J. (1998). Genetic regulation of entry into meiosis in Caenorhabditis elegans. *Development* **125**, 1803-1813. doi:10.1242/dev.125.10.1803
Kandachar, V. and Roegiers, F. (2012). Endocytosis and control of Notch signaling. *Curr. Opin. Cell Biol.* **24**, 534-540. doi:10.1016/j.ceb.2012.06.006
Kang, J., Bai, Z., Zegarek, M. H., Grant, B. D. and Lee, J. (2011). Essential roles of snap-29 in C. elegans. *Dev. Biol.* **355**, 77-88. doi:10.1016/j.ydbio.2011.04.013
Kershner, A. M., Shin, H., Hansen, T. J. and Kimble, J. (2014). Discovery of two GLP-1/Notch target genes that account for the role of GLP-1/Notch signaling in stem cell maintenance. *Proc. Natl. Acad. Sci. USA* **111**, 3739-3744. doi:10.1073/pnas.1401861111
Kimble, J. and Crittenden, S. L. (2005). Germline proliferation and its control (ed. The C. elegans Research Community), *WormBook* doi:10.1895/wormbook.1.13.1, http://www.wormbook.org
Kimble, J. and Simpson, P. (1997). The LIN-12/Notch signaling pathway and its regulation. *Annu. Rev. Cell Dev. Biol.* **13**, 333-361. doi:10.1146/annurev.cellbio.13.1.333
Kimble, J., Crittenden, S., Lambie, E., Kodoyianni, V., Mango, S. and Troemel, E. (1992). Regulation of induction by GLP1, and localized cell surface receptor in Caenorhabditis elegans. *Cold Spring Harb. Symp. Quant. Biol.* **57**, 401-407. doi:10.1101/SQB.1992.057.01.045
Kocsisova, Z., Kornfeld, K. and Schedl, T. (2019). Rapid population-wide declines in stem cell number and activity during reproductive aging in C. elegans. *Development* **146**, dev173195. doi:10.1242/dev.173195
Kodoyianni, V., Maine, E. M. and Kimble, J. (1992). Molecular basis of loss-of-function mutations in the glp-1 gene of Caenorhabditis elegans. *Mol. Biol. Cell* **3**, 1199-1213. doi:10.1091/mbc.3.11.1199
Kopan, R. and Ilagan, M. X. G. (2009). The canonical Notch signaling pathway: unfolding the activation mechanism. *Cell* **137**, 216-233. doi:10.1016/j.cell.2009.03.045
Kumar, H., Pushpa, K., Kumari, A., Verma, K., Pergu, R. and Mylavarapu, S. V. S. (2019). The exocyst complex and Rab5 are required for abscission by localizing ESCRT III subunits to the cytokinetic bridge. *J. Cell Sci.* **132**, jcs226001. doi:10.1242/jcs.226001
Kumsta, C. and Hansen, M. (2012). C. elegans rrf-1 mutations maintain RNAi efficiency in the soma in addition to the germline. *PLoS ONE* **7**, e35428. doi:10.1371/journal.pone.0035428
Lalli, G. (2009). RalA and the exocyst complex influence neuronal polarity through PAR-3 and aPKC. *J. Cell Sci.* **122**, 1499-1506. doi:10.1242/jcs.044339
Lang, C. F. and Munro, E. (2017). The PAR proteins: from molecular circuits to dynamic self-stabilizing cell polarity. *Development* **144**, 3405-3416. doi:10.1242/dev.139063
Langevin, J., Morgan, M. J., Rossé, C., Racine, V., Sibarita, J.-B., Aresta, S., Murthy, M., Schwarz, T., Camonis, J. and Bellaïche, Y. (2005). Drosophila exocyst components Sec5, Sec6, and Sec15 regulate DE-Cadherin trafficking from recycling endosomes to the plasma membrane. *Dev. Cell* **9**, 365-376. doi:10.1016/j.devcel.2005.07.013
Lant, B., Yu, B., Goudreault, M., Holmyard, D., Knight, J. D. R., Xu, P., Zhao, L., Chin, K., Wallace, E., Zhen, M. et al. (2015). CCM-3/STRIPAK promotes seamless tube extension through endocytic recycling. *Nat. Commun.* **6**, 6449. doi:10.1038/ncomms7449
Li, H., Koo, Y., Mao, X., Sifuentes-Dominguez, L., Morris, L. L., Jia, D., Miyata, N., Faulkner, R. A., van Deursen, J. M., Vooijs, M. et al. (2015). Endosomal sorting of Notch receptors through COMMD9-dependent pathways modulates Notch signaling. *J. Cell Biol.* **211**, 605-617. doi:10.1083/jcb.201505108
Linden, L. M., Gordon, K. L., Pani, A. M., Payne, S. G., Garde, A., Burkholder, D., Chi, Q., Goldstein, B. and Sherwood, D. R. (2017). Identification of regulators of germ stem cell enwrapment by its niche in C. elegans. *Dev. Biol.* **429**, 271-284. doi:10.1016/j.ydbio.2017.06.019
Liu, J. and Guo, W. (2012). The exocyst complex in exocytosis and cell migration. *Protoplasma* **249**, 587-597. doi:10.1007/s00709-011-0330-1
Liu, J., Sato, C., Cerletti, M. and Wagers, A. (2010). Notch signaling in the regulation of stem cell self-renewal and differentiation. *Curr. Top. Dev. Biol.* **92**, 367-409. doi:10.1016/S0070-2153(10)92012-7
Maddox, A. S., Habermann, B., Desai, A. and Oegema, K. (2005). Distinct roles for two C. elegans anillins in the gonad and early embryo. *Development* **132**, 2837-2848. doi:10.1242/dev.01828
Mao, Y., Tu, R., Huang, Y., Mao, D., Yang, Z., Lau, P. K., Wang, J., Ni, J., Guo, Y. and Xie, T. (2019). The exocyst functions in niche cells to promote germline stem cell differentiation by directly controlling EGFR membrane trafficking. *Development* **146**, dev174615. doi:10.1242/dev.174615
Maritzen, T., Schachtner, H. and Legler, D. F. (2015). On the move: endocytic trafficking in cell migration. *Cell. Mol. Life Sci.* **72**, 2119-2134. doi:10.1007/s00018-015-1855-9
McKay, H. F. and Burgess, D. R. (2011). 'Life is a highway': membrane trafficking during cytokinesis. *Traffic* **12**, 247-251. doi:10.1111/j.1600-0854.2010.01139.x
Mei, K., Li, Y., Wang, S., Shao, G., Wang, J., Ding, Y., Luo, G., Yue, P., Liu, J.-J., Wang, X. et al. (2018). Cryo-EM structure of the exocyst complex. *Nat. Struct. Mol. Biol.* **25**, 139-146. doi:10.1038/s41594-017-0016-2
Naegeli, K. M., Hastie, E., Garde, A., Wang, Z., Keeley, D. P., Gordon, K. L., Pani, A. M., Kelley, L. C., Morrissey, M. A., Chi, Q. et al. (2017). Cell invasion in vivo via rapid exocytosis of a transient lysosome-derived membrane domain. *Dev. Cell* **43**, 403-417.e410. doi:10.1016/j.devcel.2017.10.024
Nance, J. and Zallen, J. A. (2011). Elaborating polarity: PAR proteins and the cytoskeleton. *Development* **138**, 799-809. doi:10.1242/dev.053538
Neto, H., Kaupisch, A., Collins, L. L. and Gould, G. W. (2013a). Syntaxin 16 is a master recruitment factor for cytokinesis. *Mol. Biol. Cell* **24**, 3663-3674. doi:10.1091/mbc.e13-06-0302
Neto, H., Balmer, G. and Gould, G. (2013b). Exocyst proteins in cytokinesis: Regulation by Rab11. *Commun. Integr. Biol.* **6**, e27635. doi:10.4161/cib.27635
Pal, S., Lant, B., Yu, B., Tian, R., Tong, J., Krieger, J. R., Moran, M. F., Gingras, A.-C. and Derry, W. B. (2017). CCM-3 promotes C. elegans germline development by regulating vesicle trafficking cytokinesis and polarity. *Curr. Biol.* **27**, 868-876. doi:10.1016/j.cub.2017.02.028
Pazdernik, N. and Schedl, T. (2013). Introduction to germ cell development in Caenorhabditis elegans. *Adv. Exp. Med. Biol.* **757**, 1-16. doi:10.1007/978-1-4614-4015-4_1

Pepper, A. S.-R., Killian, D. J. and Hubbard, E. J. A. (2003). Genetic analysis of Caenorhabditis elegans glp-1 mutants suggests receptor interaction or competition. *Genetics* **163**, 115-132. doi:10.1093/genetics/163.1.115

Phillips-Krawczak, C. A., Singla, A., Starokadomskyy, P., Deng, Z., Osborne, D. G., Li, H., Dick, C. J., Gomez, T. S., Koenecke, M., Zhang, J.-S. et al. (2015). COMMD1 is linked to the WASH complex and regulates endosomal trafficking of the copper transporter ATP7A. *Mol. Biol. Cell* **26**, 91-103. doi:10.1091/mbc.e14-06-1073

Polgar, N. and Fogelgren, B. (2018). Regulation of cell polarity by exocyst-mediated trafficking. *Cold Spring Harb. Perspect. Biol.* **10**, a031401. doi:10.1101/cshperspect.a031401

Rosse, C., Formstecher, E., Boeckeler, K., Zhao, Y., Kremerskothen, J., White, M. D., Camonis, J. H. and Parker, P. J. (2009). An aPKC-exocyst complex controls paxillin phosphorylation and migration through localised JNK1 activation. *PLoS Biol.* **7**, e1000235. doi:10.1371/journal.pbio.1000235

Sato, K., Norris, A., Sato, M. and Grant, B. D. (2014). C. elegans as a model for membrane traffic (ed. The C. elegans Research Community). *WormBook* doi:10.1895/wormbook.1.77.2, http://www.wormbook.org

Schnute, B., Troost, T. and Klein, T. (2018). Endocytic trafficking of the Notch receptor. *Adv. Exp. Med. Biol.* **1066**, 99-122. doi:10.1007/978-3-319-89512-3_6

Sharma, A., Dagar, S. and Mylavarapu, S. V. S. (2020). Transgelin-2 and phosphoregulation of the LIC2 subunit of dynein govern mitotic spindle orientation. *J. Cell Sci.* **133**, jcs239673. doi:10.1242/jcs.239673

Shin, H., Haupt, K. A., Kershner, A. M., Kroll-Conner, P., Wickens, M. and Kimble, J. (2017). SYGL-1 and LST-1 link niche signaling to PUF RNA repression for stem cell maintenance in Caenorhabditis elegans. *PLoS Genet.* **13**, e1007121. doi:10.1371/journal.pgen.1007121

Siebel, C. and Lendahl, U. (2017). Notch Signaling in Development, Tissue Homeostasis, and Disease. *Physiol. Rev.* **97**, 1235-1294. doi:10.1152/physrev.00005.2017

Sommer, B., Oprins, A., Rabouille, C. and Munro, S. (2005). The exocyst component Sec5 is present on endocytic vesicles in the oocyte of Drosophila melanogaster. *J. Cell Biol.* **169**, 953-963. doi:10.1083/jcb.200411053

Sorensen, E. B., Seidel, H. S., Crittenden, S. L., Ballard, J. H. and Kimble, J. (2020). A toolkit of tagged glp-1 alleles reveals strong glp-1 expression in the germline, embryo, and spermatheca. *MicroPubl Biol.* doi:10.17912/micropub.biology.000271

Suh, N., Crittenden, S. L., Goldstrohm, A., Hook, B., Thompson, B., Wickens, M. and Kimble, J. (2009). FBF and its dual control of gld-1 expression in the Caenorhabditis elegans germline. *Genetics* **181**, 1249-1260. doi:10.1534/genetics.108.099440

Takahashi, S., Kubo, K., Waguri, S., Yabashi, A., Shin, H.-W., Katoh, Y. and Nakayama, K. (2012). Rab11 regulates exocytosis of recycling vesicles at the plasma membrane. *J. Cell Sci.* **125**, 4049-4057. doi:10.1242/jcs.102913

Taylor, C. A., Yan, J., Howell, A. S., Dong, X. and Shen, K. (2015). RAB-10 regulates dendritic branching by balancing dendritic transport. *PLoS Genet.* **11**, e1005695. doi:10.1371/journal.pgen.1005695

Tijsterman, M., Okihara, K. L., Thijssen, K. and Plasterk, R. H. A. (2002). PPW-1, a PAZ/PIWI protein required for efficient germline RNAi, is defective in a natural isolate of C. elegans. *Curr. Biol.* **12**, 1535-1540. doi:10.1016/S0960-9822(02)01110-7

Timmons, L. and Fire, A. (1998). Specific interference by ingested dsRNA. *Nature* **395**, 854. doi:10.1038/27579

Tojima, T. and Kamiguchi, H. (2015). Exocytic and endocytic membrane trafficking in axon development. *Dev. Growth Differ.* **57**, 291-304. doi:10.1111/dgd.12218

van Ijzendoorn, S. C. D. (2006). Recycling endosomes. *J. Cell Sci.* **119**, 1679-1681. doi:10.1242/jcs.02948

Wan, P., Zheng, S., Chen, L., Wang, D., Liao, T., Yan, X. and Wang, X. (2019). The exocyst component Sec3 controls egg chamber development through Notch during Drosophila oogenesis. *Front. Physiol.* **10**, 345. doi:10.3389/fphys.2019.00345

Winter, J. F., Höpfner, S., Korn, K., Farnung, B. O., Bradshaw, C. R., Marsico, G., Volkmer, M., Habermann, B. and Zerial, M. (2012). Caenorhabditis elegans screen reveals role of PAR-5 in RAB-11-recycling endosome positioning and apicobasal cell polarity. *Nat. Cell Biol.* **14**, 666-676. doi:10.1038/ncb2508

Wu, B. and Guo, W. (2015). The exocyst at a glance. *J. Cell Sci.* **128**, 2957-2964. doi:10.1242/jcs.156398

Yamamoto, S., Charng, W.-L. and Bellen, H. J. (2010). Endocytosis and intracellular trafficking of Notch and its ligands. *Curr. Top. Dev. Biol.* **92**, 165-200. doi:10.1016/S0070-2153(10)92005-X

Yang, J., Guo, W., Wang, L., Yu, L., Mei, H., Fang, S., Chen, A., Liu, Y., Xia, K. and Liu, G. (2017). Notch signaling is important for epithelial-mesenchymal transition induced by low concentrations of doxorubicin in osteosarcoma cell lines. *Oncol. Lett.* **13**, 2260-2268. doi:10.3892/ol.2017.5708

Zhang, X.-M., Ellis, S., Sriratana, A., Mitchell, C. A. and Rowe, T. (2004). Sec15 is an effector for the Rab11 GTPase in mammalian cells. *J. Biol. Chem.* **279**, 43027-43034. doi:10.1074/jbc.M402264200

Zhou, K., Rolls, M. M. and Hanna-Rose, W. (2013). A postmitotic function and distinct localization mechanism for centralspindlin at a stable intercellular bridge. *Dev. Biol.* **376**, 13-22. doi:10.1016/j.ydbio.2013.01.020

Zhu, Y., Wu, B. and Guo, W. (2017). The role of Exo70 in exocytosis and beyond. *Small GTPases* **10**, 331-335. doi:10.1080/21541248.2017.1328998

Zou, W., Yadav, S., DeVault, L., Nung Jan, Y. and Sherwood, D. R. (2015). RAB-10-dependent membrane transport is required for dendrite arborization. *PLoS Genet.* **11**, e1005484. doi:10.1371/journal.pgen.1005484

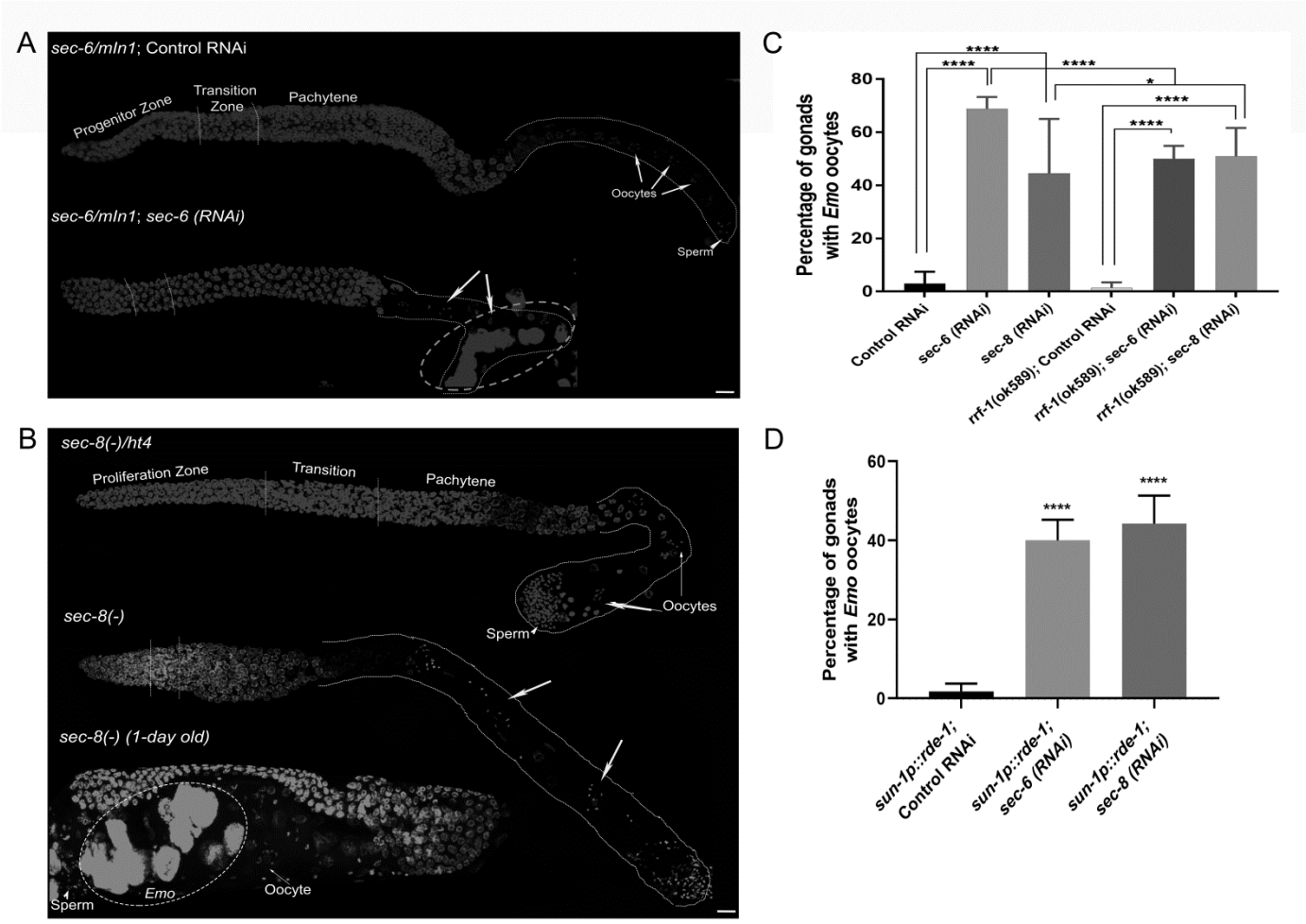

Fig. S1. Genetic mutants of sec-6 and sec-8 phenocopy RNAi-induced germline development defects. (A) Maximum projection fluorescence images of dissected and whole-mounted gonads from the indicated mutant adult genotypes, stained with DAPI (grey). **(B)** Maximum projection fluorescence images of dissected and whole mounted gonads from the indicated genotypes, stained with DAPI (grey) at young and 1-day old adult. Dashed oval marks endoreduplicating (*emo*) oocytes. For both panels: dotted vertical lines demarcate the transition zone (TZ) from the progenitor zone (PZ) and pachytene (meiotic zone); dotted trace curves outline the proximal gonadal boundary. **(C, D)** Fraction of gonads showing endoreduplicating (Emo) oocytes upon exocyst subunit RNAi in wild type (n > 80 worms) and *rrf-1* mutant worms (n >120 worms) (D) and sun-1p::rde-1 (n >100 worms). Arrows = oocytes, arrowhead = sperm. Scale bar = 20 µm.

Development • Supplementary information

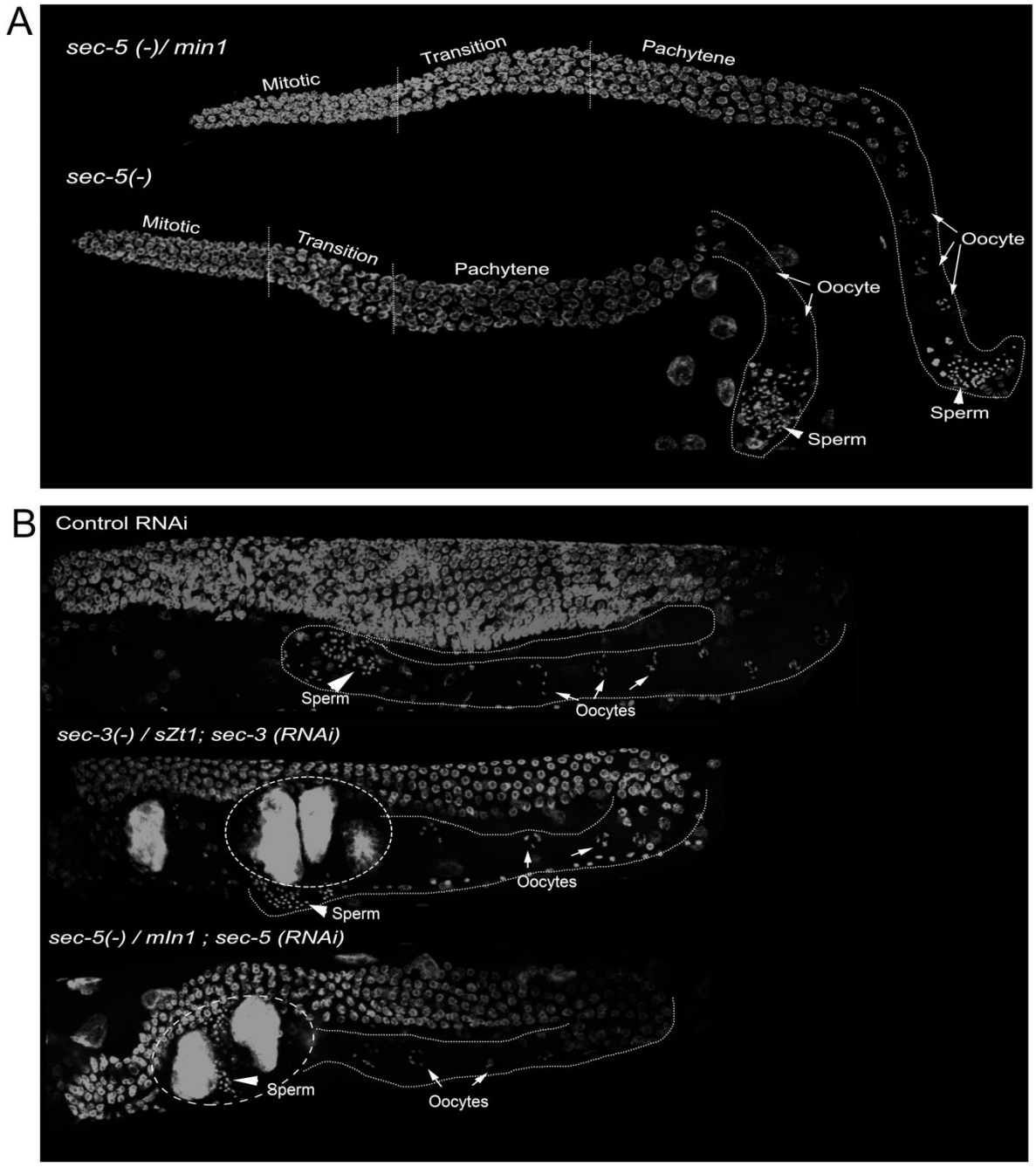

Fig. S2. Exocyst complex components sec-3 and sec-5 are required for germline development in C. elegans. (A) Maximum projection fluorescence images of dissected and whole-mounted gonads from the indicated mutant adult genotypes, stained with DAPI (grey). **(B)** Whole-mounted maximum projection images of hermaphrodite gonads stained with DAPI (grey) from the indicated genotypes. Dashed ovals mark endoreduplicating (*emo*) oocytes. For both panels: dotted vertical lines demarcate the transition zone from the progenitor zone (PZ) and pachytene (meiotic zone); dotted trace curves outline the proximal gonadal boundary. Arrows = oocytes, arrowheads = sperm. Scale bar = 20 µm

Development • Supplementary information

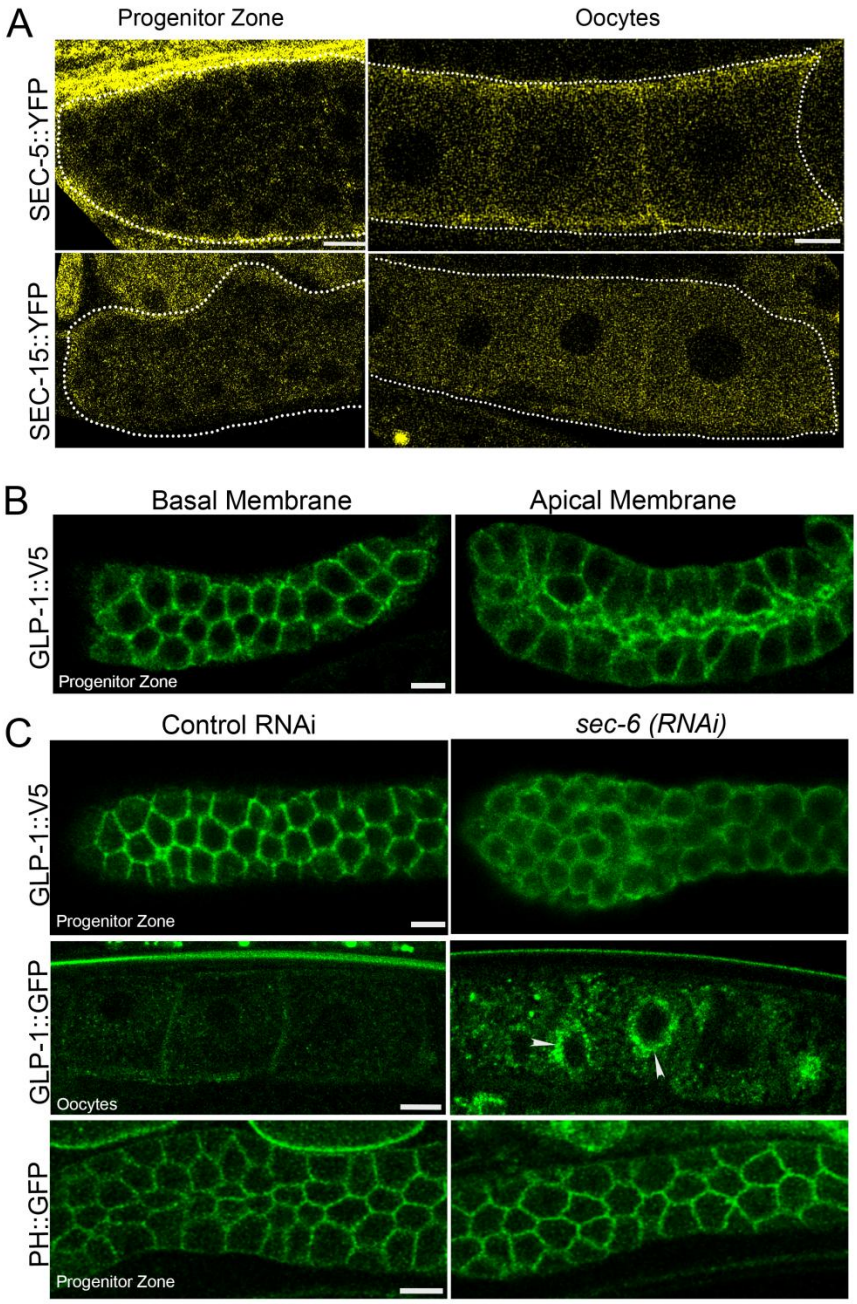

Fig. S3. The Exocyst complex is expressed in the germline and is required for trafficking of GLP-1 in the germline. (A) Representative confocal micrographs of the progenitor zone (PZ) and oocytes expressing SEC-5::YFP and SEC-15::YFP. **(B)** Representative immunofluorescence micrographs of dissected hermaphrodite gonads expressing the GLP-1::V5 transgene, stained with an anti-V5 antibody showing the outer and inner membranes (top panel) of the PZ and gonads subjected to RNAi as indicated (bottom panel). **(C)** Representative confocal fluorescence micrographs of GLP-1::V5 immunostaining on the outer membrane of GSCs (upper panel), GLP-1::GFP in oocytes (middle panel) and PH::GFP, a plasma membrane marker (bottom panel) in control and *sec-6 RNAi* Scale bar = 10 µm

Development • Supplementary information

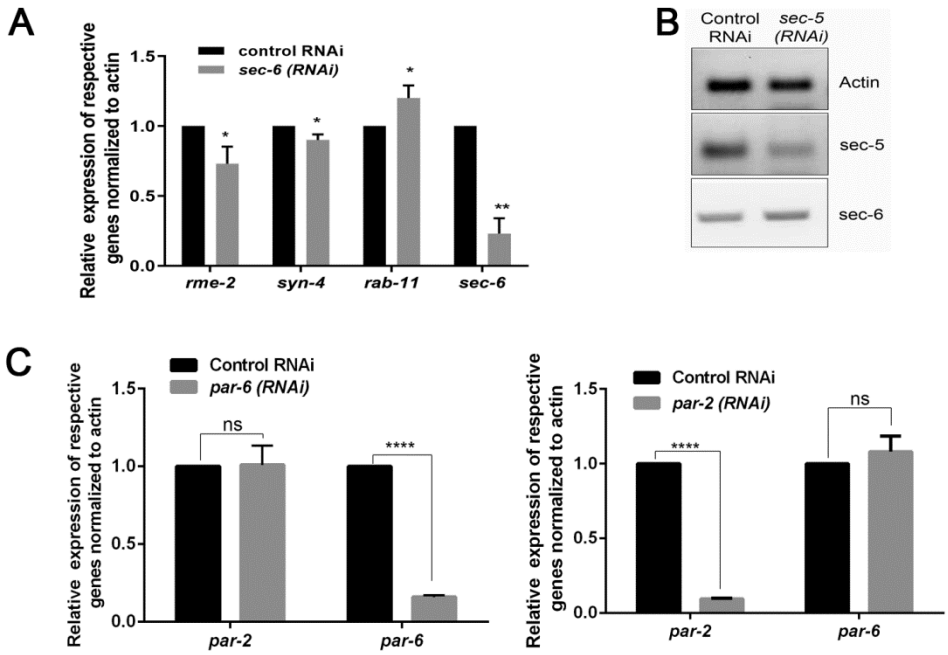

Fig. S4. A. Quantitative RT-PCR analysis of the indicated genes in the respective RNAi backgrounds. A) Relative gene expression of rme-2, syn-4, rab-11 and sec-6 upon control and sec-6 RNAi. **B))** Agarose gels showing the specific reduction in levels of the indicated genes in control and sec-5 (RNAi) using a semi-quantitative RT-PCR as compared to the β-actin control. **C)** Relative mRNA expression of par-6 and par-2 in the respective RNAi backgrounds, indicating the specificity of the RNAi.

Development • Supplementary information

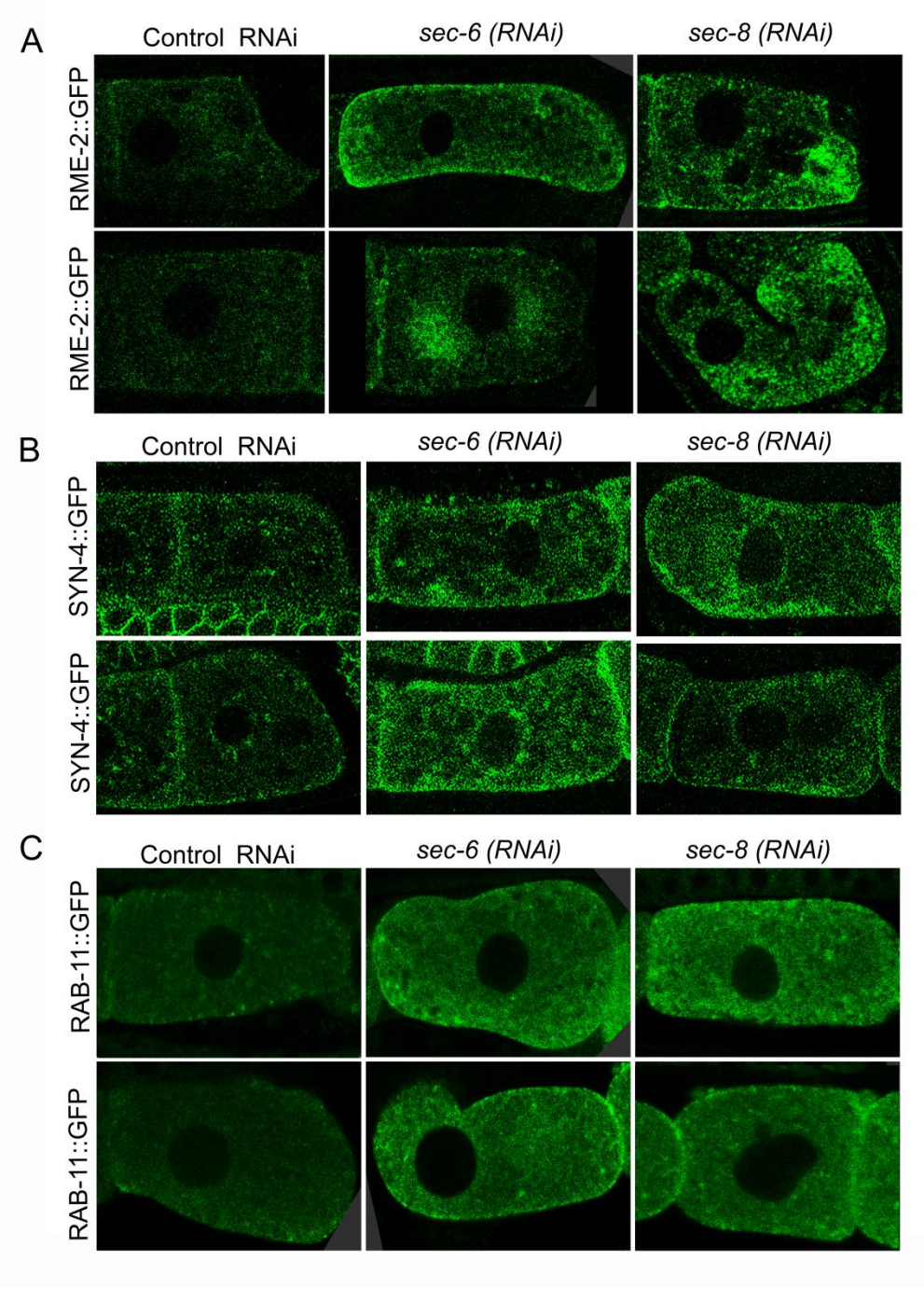

Fig. S5. The Exocyst complex is required for vesicular trafficking in C. elegans oocytes*:* Confocal fluorescence micrographs of mature oocytes expressing the indicated tagged protein RME-2::GFP **(A)**, SYN-4::GFP **(B)** and RAB-11::GFP **(C)** upon control, *sec-6* or *sec-8 (RNAi)*.

Development • Supplementary information

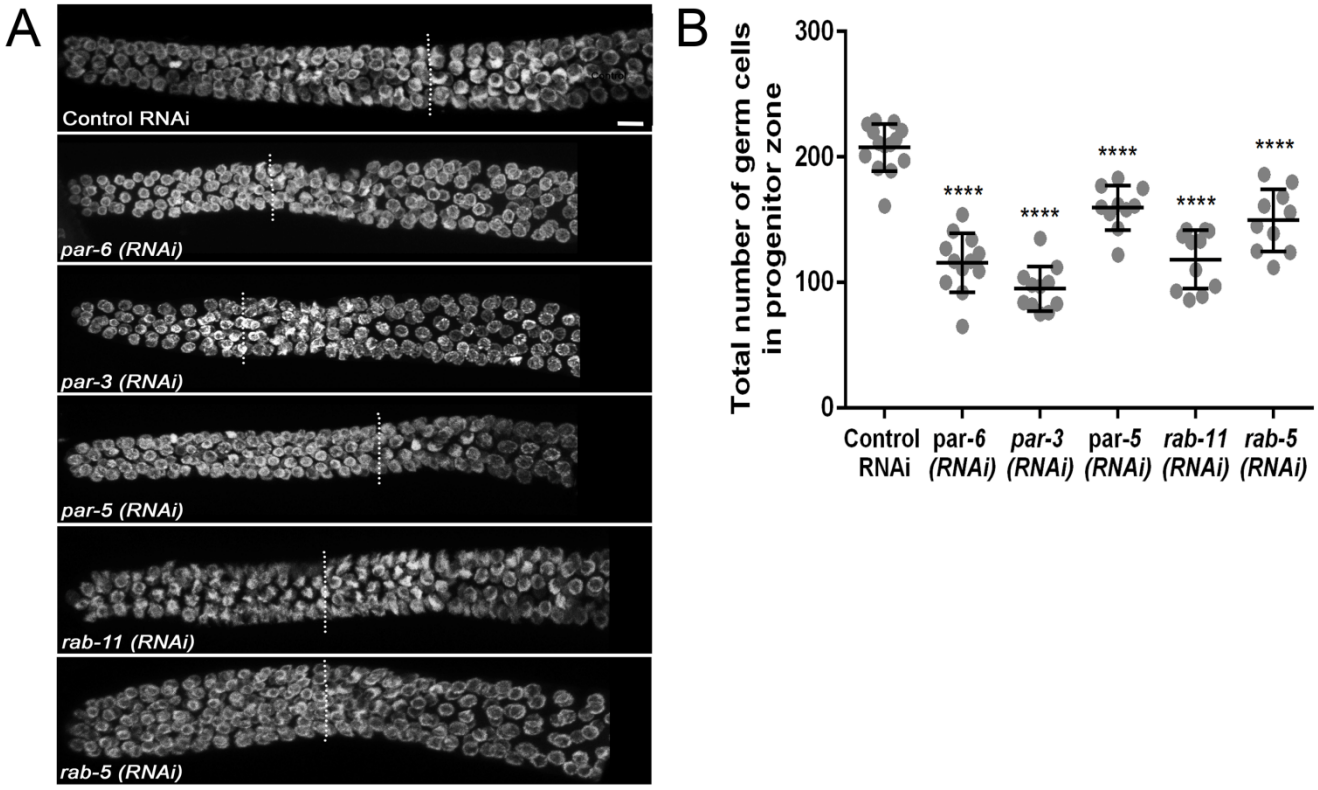

Fig. S6. Germline stem cell proliferation is defective upon RNAi of aPars and Rab GTPases Rab-5 and Rab-11: A) Representative confocal immunofluorescence micrographs of dissected hermaphrodite gonads from the indicated RNAi and stained with the DNA-binding dye (grey, DAPI). Dashed line demarcates the progenitor zone (PZ) from the transition zone (TZ). **B)** Total number of GSCs upon knockdown of the indicated genes. Scale bar = 10 µm.

Development • Supplementary information

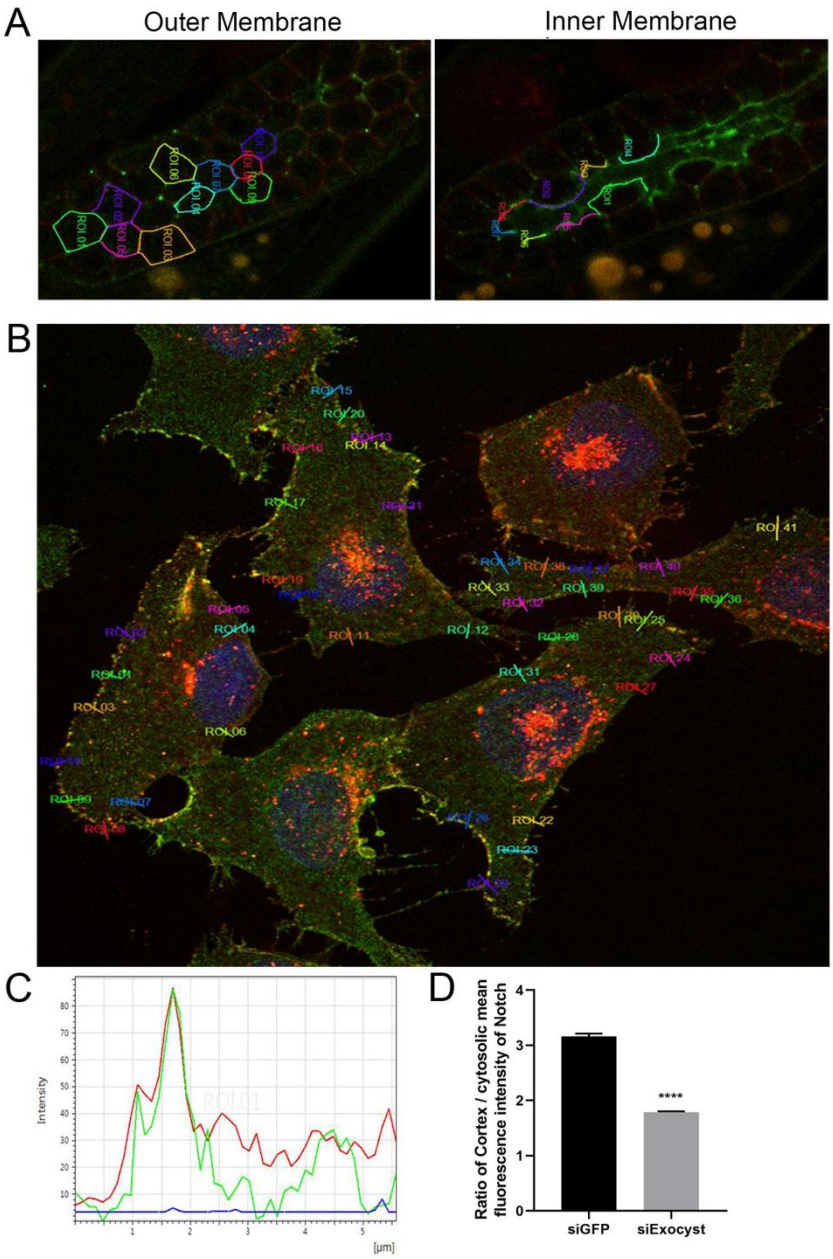

Fig. S7. Pictorial representation of methodology for drawing line scans to quantify plasma membrane levels of Notch in C. elegans and mammalian cells. **(A)** Representative micrographs of the progenitor zone (PZ) from animals expressing GLP-1::GFP (green) and PH::mCherry (red) showing the merged image (green + red). Linescans were drawn on images of a single confocal plane that corresponded to the top (for the outer surface) and middle (for the inner surface) focal plane of the gonad along the cell boundaries using red fluorescence (PH::mCherry, which decorates the plasma membrane) as a guide and the mean fluorescence intensity of the green channel (GLP-1::GFP) was calculated using LASX software analysis tool (see Materials and Methods). About 8-10 cells per gonad from 12-15 worms (one gonadal arm/worm) were used for these measurements. **(B)** Representative

Development • Supplementary information

max projection image of a field of mammalian cells (U2OS) co-stained with wheat-germ agglutinin (WGA – red) and human Notch2 (green). Linescans were drawn across the cell boundary from outside the cell to the cytoplasm using WGA (red) staining as the guide for the plasma membrane. Since the WGA staining was not uniform throughout, only the well-stained regions of the cell boundary were used to draw the linescans. Peak fluorescence intensity on the membrane in the green channel (for Notch2) was measured using the red channel (WGA) membrane peak as the guide. A minimum of 5 ROIs for each cell and about 40-50 ROIs per field were drawn. From a single field, only 5 cells were used for analysis to avoid over representation and uniform and unbiased data collection. **(C)** Graph shows the peak intensity at a given point on the line scan. We analyzed the peak intensity in the green channel corresponding to the plasma membrane falling within a 2 nm region of the red peak **(D)** Fraction of cortical and cytoplasmic Notch2 receptor (see Materials and Methods for details) upon control and exocyst complex siRNA treatment in U2OS cells.

Development • Supplementary information

A

Yeast two-hybrid		
Serial Number	Gene Name	PBS* score
1	SEC-5	**A**
2	PAR-5	**C**
3	KLC-1	**C**
4	PGL-3	**D**
5	UNC-15	**A**

PBS score: Predicted Biological Score, a confidence score attributed to interactions as described in Formstecher et al., 2005.
A: Very high confidence
B: High confidence
C: Good interaction
D. Moderate interaction
E. Highly connected interaction, due to highly interactive or connected proteins or promiscuous domains
F. Technical artifacts

B

Mass spectrometry			
Serial Number	**Gene Name**	**Number of peptides**	**% Coverage**
1	SEC-3	7	15.9
2	SEC-5	1	3.7
3	SEC-8	4	8.7
4	RAB-11	1	16.5
5	PAR-5	12	54.8
6	KLC-2	2	9.6
7	PGL-1	4	9.3
8	UNC-15	3	6.3

Fig. S8. PAR5 is identified as an interactor of exocyst subunit SEC6/ Exoc3 from C. elegans and human systems. (**A)** Selected high confidence interactors of exocyst subunit SEC-6 from *C. elegans* obtained through a yeast two-hybrid screen. See Materials and Methods for details. (**B)** Selected high confidence interactors of exocyst subunit Sec-6 from whole worm lysates expressing SEC-6::GFP::SBP, obtained through affinity purification using SBP-tag followed by mass spectrometry. See Materials and Methods for details.

Development • Supplementary information

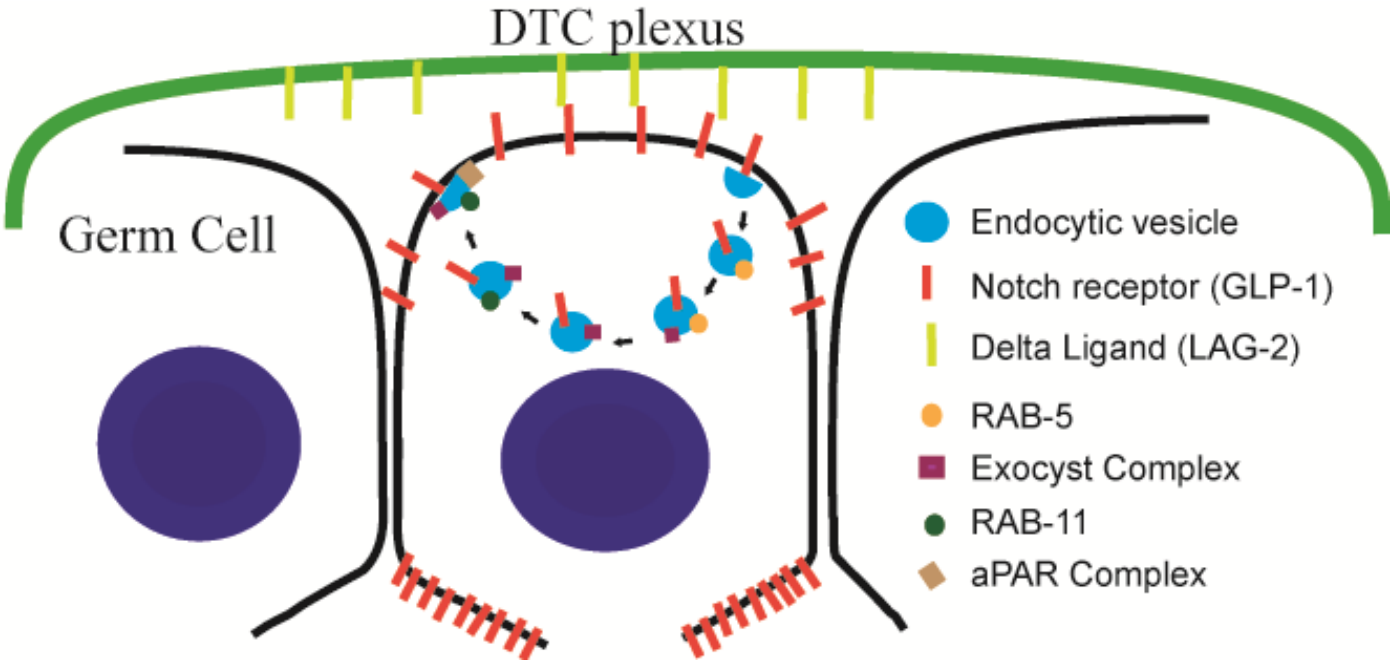

Fig. S9. Graphical model representing Notch/GLP-1 distribution in the GSCs in C. elegans and a possible mechanism of Notch trafficking and localization at the Niche-facing membrane of GSCs by Exocyst complex, Rab GTPases RAB-5, RAB-11 and aPar complex.

Development • Supplementary information

Table S1. Description of strains used in this study

Strain Name	Description	Source
N2	Bristol strain, Wild type	CGC
OD95	ltIs37[(pAA64) pie-1p::mCherry::his-58 + unc-119(+)] IV; ltIs38 [pie-1p::GFP::PH (PLC1delta1) + unc-119(+)]	CGC
OD70	ltIs44 [pie-1p::mCherry::PH(PLC1delta1) + unc-119(+)]	CGC
OD58	ltIs38 [pie-1p::GFP::PH(PLC1delta1) + unc-119(+)]	CGC
RT368	unc-119(ed3) III; pwIs98 [YP170::tdimer-2; unc-119 (+)]	CGC
VC2648	sec-8(ok2187) I/hT2 [bli-4(e937) let-?(q782) qIs48] (I;III)	CGC
tm4536	sec-6(tm4536) /mIn1 [mIs14 dpy-10(e128)] II	NBRP
DV2689	sec-5(pk2358)/ mIn1 [dp-10(e128) mIs14] II	CGC
VC2003	+/szT1[lon-2(e678)] I; sec-3(ok2238)/szT1 X	CGC
FT1265	sec-5(pk2358)II; xnIs461 [sec-5::YFP+ unc-119(+)]	CGC
FT1379	avr-14(ad1302) I; xnSi34 [sec-15::YFP+ Unc-119(+)] II; unc-119 (ed3) III; glc-1(pk54::Tc1) avr-15(ad1051) V	CGC
WH327	ojIs23 [pie-1p::GFP::C34B2.10]	CGC
RB798	rrf-1(ok589) I.	CGC
WH351	ojIs37 [pie-1p::GFP::ugtp-1 + unc-119(+)]	CGC
WH347	unc-119(ed3) III; ojIs35 [pie-1p::GFP::rab-11.1; unc-119 (+)]	CGC
GC833	glp-1(ar202) III	CGC
DG2389	glp-1(bn18) III	CGC
MVS1	sec-6 (SMYL04[sec-6::GFP::SBP] II	This study
MVS6	sec-6 (SMYL04[sec-6::GFP::SBP] II; ltIs44 [pie-1p::mCherry::PH (PLC1delta1) + unc-119(+)]	This study
MVS8	EV343; ltIs44 [pie-1p::mCherry::PH (PLC1delta1) + unc-119(+)]	This study
JK2868	qIs56 [lag-2p::GFP + unc-119(+)]	CGC
JH2060	axIs1498 [pie-1p::GFP::gld-1 ORF::gld-1 3'utr + unc-119(+)]	CGC
EV343	efEx12 [glp-1::TY1::EGFP::3xFLAG(92C12) + unc-119(+)]	CGC
RT408	pwIs116 [rme-2p::rme-2::GFP::rme-2 3'UTR + unc-119(+)].	CGC
JK5933	glp-1(q1000[glp-1::4xV5]) III.	Kimble Lab
JK5929	lst-1(q1004[lst-1::4XV5]) I	CGC
JK6002	sygl-1(q1004[sygl-1::4XV5]) I	CGC
MVS 10	sec-6 (SMYL04[sec-6::GFP::SBP] II; efEx12 [glp-1::TY1::EGFP::3xFLAG(92C12) + unc-119(+)]	This study
MVS 11	sec-6 (SMYL05[sec-6::degron::GFP::SBP] II	This study
CA1199	ieSi38 [sun-1p::TIR1::mRuby::sun-1 3'UTR + Cbr-unc-119(+)] IV.	CGC
MVS12	sec-6 (SMYL05[sec-6::degron::GFP::SBP] II; CA1199 (ieSi38 [sun-1p::TIR1::mRuby::sun-1 3'UTR + Cbr-unc-119(+)] IV.)	This study
DCL569	mkcSi13 [sun-1p::rde-1::sun-1 3'UTR + unc-119(+)] II.	CGC
JK2879	gld-2(q497) gld-1(q485)/hT2 [bli-4(e937) let-?(q782) qIs48] (I;III)	CGC
JK3182	gld-3(q730) nos-3(q650)/mIn1 [mIs14 dpy-10(e128)] II	CGC

Development • Supplementary information

Table S2. Description of oligos used in this study

Oligo name	Sequence	Purpose
PK1	TCTAAGCTTTAGCAGTCACAATCGAGCAC	Forward to clone sec-3 in RNAi vector
PK2	TCTAAGCTTCGAGAGATTGCAATTGCTCC	Reverse to clone sec-3 in RNAi vector
PK3	TCTAAGCTTACTACCTCCTACGGTAACAG	Forward to clone sec-5 in RNAi vector
PK4	TCTAAGCTTGCGTCTGCATGATTCTCTAG	Reverse to clone sec-5 in RNAi vector
PK5	TCTAAGCTTTGGACGTTGATGTGGAAGAG	Forward to clone sec-6 in RNAi vector
PK6	TCTAAGCTTGAACTTCGGCCAGCAATTCG	Reverse to clone sec-6 in RNAi vector
PK7	TCTCCCGGGCTAGAAGGCATCGACCATTG	Forward to clone sec-8 in RNAi vector
PK8	TCTCCCGGGTCCACTCGTGATAATCGTCC	Reverse to clone sec-8 in RNAi vector
MVS136	TCCGAGAATCTTCCTAATTGAAAT	Forward to detect rrf-1(ok589) deletion
MVS138	TCGAAGGGATTCAATTCGTC	Reverse to detect rrf-1(ok589) deletion
PK17	GTGGAACAAATGCCGATGAG	Forward to detect sec-6(tm4536) deletion
PK38	TCTGAGGGATCCATGGACGTTGATGTGGAAGAG	Forward to detect sec-6(tm4536) deletion
MVS395	AACTTCAAAATTAGACACAACATTGAAGAT	Forward to detect SEC-6::GFP Crisper-edit
MVS396	AGTCAGCTTTGAACATGTTGGC	Reverse to detect SEC-6::GFP Crisper-edit
MVS393	CAGACACAGATGTTCCGTTG	Fwd in Sec-5(pk2358) ahead of mutation
MVS392	GAGAAAAGTCTCTGGGATATGT	Fwd to detect Sec-5(pk2358) mutant
MVS394	GAAGAGCTTTGGGAACCAG	Reverse to detect mutation in sec-5(pk2358)
MVS389	GTACTGGGAACTGCAAGCAG	Forward to detect Sec-8 deletion
MVS390	GCAGGAGAAGACAAGAATCAGC	Fwd to detect Sec-8 deletion
MVS499	AAGCTGGTGTCGCGTGTATG	Forward for rme-2 RT-PCR
MVS500	ATGACTCCAGCGAATGGTGC	Reverse for rme-2 RT-PCR
MVS508	CTCTCGTGACGATGAATACGAC	Forward for rab-11.1 RT-PCR
MVS509	CACTGTCTTGCCTTCTACCG	Reverse for rab-11.1 RT-PCR
MVS510	CGCAGATCGACACGCAATTT	Forward for syn-4 RT-PCR
MVS511	ATGCCACGTGCTTGAGCTAT	Reverse for syn-4 RT-PCR
MVS512	CGGAGAGGAGCAAGTATCAAGAG	Forward for Sec-6 RT-PCR
MVS513	TACGTCGTCCTGATGCGAGT	Reverse for Sec-6 RT-PCR
MVS514	CGTTTTGGAGATCCGCTCAG	Forward for Sec-8 RT-PCR
MVS515	TCTGCTTGCAGTTCCCAGTA	Reverse for Sec-8 RT-PCR
MVS516	CGATTCGTGATGTGTGTGCT	Forward for Par-2 RT-PCR
MVS517	GGTGATGACGTGGGAGTTTG	Reverse for Par-2 RT-PCR
MVS518	TTCTCGGAAAGACGCTGGAT	Forward for Par-6 RT-PCR
MVS519	GCTGAATTCCACCTGTAGCG	Reverse for Par-6 RT-PCR
MVS520	CCGCTCTTGCCCCATCAACCATG	Forward for actin RT-PCR
MVS521	CGGACTCGTCGTATTCTTGCT	Reverse for actin RT-PCR
MVS534	GGCTCTCTCAACGTATGCCA	Forward for Sec-5 RT-PCR
MVS535	TCGCATAGTGGTTCGCATGT	Reverse for Sec-5 RT-PCR
MVS522	GGCTGTGGCCGAAGTGAT	Forward for hExoc3 RT-PCR
MVS523	CTGGATACTTGGCGTCCCC	Reverse for hExoc3 RT-PCR
MVS526	CGAGGTGGAGAAGGAGAGTG	Forward for Hey1 RT-PCR
MVS527	CTGGGTACCAGCCTTCTCAG	Reverse for Hey1 RT-PCR
MVS530	AACTGTTGGTGGCCTGAATC	Forward for Herp2 RT-PCR
MVS531	GCTGGTAAATGCAGGCGTAT	Reverse for Herp2 RT-PCR

Table S3

Click here to download Table S3

Development • Supplementary information